FENOC
FirstEnergy Nuclear Operating Company

Beaver Valley Power Station
P.O. Box 4
Shippingport, PA 15077

Paul A. Harden
Site Vice President

724-682-5234
Fax: 724-643-8069

January 5, 2011
L-10-329

10 CFR 50.90

ATTN: Document Control Desk
U. S. Nuclear Regulatory Commission
Washington, DC 20555-0001

SUBJECT:
Beaver Valley Power Station, Unit No. 2
Docket No. 50-412, License No. NPF-73
Supplemental Information for Beaver Valley Power Station Unit 2 Spent Fuel Pool Rerack License Amendment Request (TAC No. ME1079)

By correspondence dated April 9, 2009 (Reference 1), as supplemented by correspondence dated June 15, 2009 (Reference 2), January 18, 2010 (Reference 3), March 18, 2010 (Reference 4), May 3, 2010 (Reference 5), May 21, 2010 (Reference 6), June 1, 2010 (Reference 7), August 9, 2010 (Reference 8), October 7, 2010 (Reference 9), and October 18, 2010 (Reference 10) FirstEnergy Nuclear Operating Company (FENOC) requested a license amendment for Beaver Valley Power Station (BVPS), Unit No. 2. The proposed amendment would revise the Technical Specifications to support the installation of high density fuel storage racks in the BVPS, Unit No. 2 spent fuel pool (SFP).

During a September 27, 2010 public meeting, the Nuclear Regulatory Commission (NRC) staff requested information related to requests for additional information (RAI) provided in References 5, 6, and 8. A public teleconference meeting held on December 15, 2010 discussed supplemental information relevant to the aforementioned RAIs. The supplemental RAI responses are attached.

The information provided by this submittal does not invalidate the no significant hazards consideration submitted in Reference 1. There are no regulatory commitments contained in this letter. If there are any questions or if additional information is required, please contact Mr. Thomas A. Lentz, Manager – FENOC Fleet Licensing, at 330-761-6071.

A001
NRR

I declare under penalty of perjury that the foregoing is true and correct. Executed on January 5, 2011.

Sincerely,

Paul A. Harden

Attachment:
Response to September 27, 2010 NRC Request for Supplemental Information

References:

1. FENOC Letter L-09-086, "License Amendment Request No. 08-027, Unit 2 Spent Fuel Pool Rerack," dated April 9, 2009 (Accession No. ML091210251).
2. FENOC Letter L-09-162, "Additional Technical Information Pertaining to License Amendment Request No. 08-027 (TAC No. ME1079)," dated June 15, 2009 (Accession No. ML091680614).
3. FENOC Letter L-10-001, "Response to Request for Additional Information for License Amendment Request No. 08-027, Unit 2 Spent Fuel Pool Rerack (TAC No. ME1079)," dated January 18, 2010 (Accession No. ML100191805).
4. FENOC Letter L-10-082, "Response to NRC Staff Request for Additional Information Regarding Criticality Analyses Supporting a Spent Fuel Pool Re-rack for Unit 2 (TAC No. ME1079)," dated March 18, 2010 (Accession No. ML100820165).
5. FENOC Letter L-10-121, "Response to Request for Additional Information Related to Beaver Valley Power Station Unit No. 2 Spent Fuel Pool Rerack License Amendment Request (TAC No. ME1079)," dated May 3, 2010 (Accession No. ML101260059).
6. FENOC Letter L-10-151, "Response to Request for Additional Information Related to Beaver Valley Power Station Unit No. 2 Spent Fuel Pool Rerack License Amendment Request (TAC No. ME1079)," dated May 21, 2010 (Accession No. ML101460057).
7. FENOC Letter L-10-130, "Remainder of Responses to NRC Staff Request for Additional Information Regarding Unit 2 Spent Fuel Pool Rerack Criticality Analyses (TAC No. ME1079)", dated June 1, 2010 (Accession No. ML101610118).
8. FENOC Letter L-10-235, "Response to Request for Additional Information for License Amendment Request No. 08-027, Unit 2 Spent Fuel Pool Rerack (TAC No. ME 1079)," dated August 9, 2010 (Accession No. ML102240256).

9. FENOC Letter L-10-282, "Supplemental Response to Request for Additional Information Related to Beaver Valley Power Station Unit No. 2 Spent Fuel Pool Rerack License Amendment Request (TAC No. ME 1079)," dated October 7, 2010 (Accession No. ML102860124).
10. FENOC Letter L-10-275, "License Amendment Request for Unit 2 Spent Fuel Pool Rerack (TAC No. ME1079)," dated October 18, 2010 (Accession No. ML102940454).

cc: NRC Region I Administrator
NRC Senior Resident Inspector
NRC Project Manager
Director BRP/DEP
Site BRP/DEP Representative

ATTACHMENT
L-10-329

Response to September 27, 2010 NRC Request for Supplemental Information

By correspondence dated April 9, 2009, the FirstEnergy Nuclear Operating Company (FENOC) submitted to the Nuclear Regulatory Commission (NRC) a license amendment request related to the Beaver Valley Power Station, Unit No. 2 (BVPS-2) spent fuel pool storage racks. By letter dated March 19, 2010, the NRC staff requested additional information related to the license amendment request. FENOC's response to this request was provided in correspondence dated May 3, 2010 and May 21, 2010 with supplemental information related to the request for additional information (RAI) response submitted on August 9, 2010. On September 27, 2010, a public meeting was held to discuss the NRC staff's questions related to FENOC's responses to RAI numbers 5, 6, 8, 17, and 19. A public teleconference meeting was held on December 15, 2010 and discussed supplemental information relevant to the aforementioned RAIs. The questions provided by the NRC staff as a result of the September 27, 2010 public meeting are provided below in bold text and are followed by the FENOC response.

Supplement to RAI-5

1. In August 9, 2010 supplemental response, moment due to Dead Load (D) is discussed. Provide further information relative to what is included in this load case. Specifically, provide confirmation that the weight of the water is included in the base slab evaluation.

Response:

For the base slab evaluation presented in the August 9, 2010 supplemental response, the Dead Load (D) includes the self-weight of the reinforced concrete slab, the weight of the spent fuel pool (SFP) water, and the buoyant weight of the spent fuel racks plus fuel. With regard to the SFP water weight, a uniform pressure of 17.33 pounds per square inch (psi) was applied to the top surface of the SFP slab to account for the 40-foot height of water in determining the moment due to Dead Load (D). While accounting for the dead weight of the SFP contents, the response to supplemental question 3 details a strain-limited rather than a load-limited base slab evaluation.

2. The LAR states the following:

"To confirm the structural integrity of the racks, it is necessary to demonstrate compliance with the USNRC Standard Review Plan [5.1] and the OT Position Paper [5.2]." **Both Appendix D to SRP 3.8.4 and the OT position paper (GL 78-11) state that the ductility ratios utilized to absorb kinetic energy should be**

quantified. Provide further information and justify that the total strain in the base slab [strain due to the rack impact plus the existing strain in the base slab due to other loads (dead load, water load, etc.)] is within the acceptance limit determined based on the allowable ductility ratios specified in the BVPS-2 UFSAR.

Response:

The ductility ratios (μ) for reinforced concrete missile barriers are specified in Section 3.5.3 of the BVPS-2 UFSAR and bounds the allowable limits used for design, which are summarized as follows:

> Reinforced concrete – beam-column members and slabs (tension controlling) $\mu \leq 10$
> Reinforced concrete – beam-column members and slabs (compression controlling)
> $\mu \leq 1.3$
> Reinforced concrete – beams and slabs (in region requiring shear reinforcement) $\mu = 1.3$

Although the slab permissible ductility ratio is not defined in American Concrete Institute *Building Code Requirements for Reinforced Concrete* (ACI 318-71), which is the SFP design code of record, Appendix C of *American Concrete Institute Code Requirements for Nuclear Safety Related Concrete Structures* (ACI 349-85) defines it as the ratio of the maximum acceptable displacement to the displacement at the effective yield point. Since the yield point is not reached under the rack drop condition, the ductility ratio for the postulated rack drop event is less than one. Therefore, the impacted SFP slab will not violate the allowable ductility ratios specified in the BVPS-2 UFSAR.

3. Provide the basis for the value of subgrade modulus (260 kips/ft^3). In addition, provide further information and confirm that the uncertainty in the value of the subgrade modulus has been taken into account or provide justification that excluding the variation of subgrade modulus has minimal effects on the outcome of the analysis.

Response:

In the August 9, 2010 supplemental response, the presented base slab evaluation applied a subgrade modulus of 260 kips/ft^3 based on an investigative study performed by Stone & Webster in 1976. The LS-DYNA model in the alternative evaluation presented below conservatively ignores the presence of the SFP slab subgrade material.

Based on engineering judgment that a rack drop accident will not cause a global structural failure of the SFP slab, the initial rack drop analysis was intended to analyze the structural integrity of the SFP floor liner and to evaluate the local damage of the SFP concrete slab. Therefore, only a small region (55.25" long × 55.25" wide × 24" thick) of the slab adjacent to the impact location was considered in the model. To obtain a quantitative assessment of the SFP slab global behavior under the rack drop condition, a revised rack drop analysis that yields both local and global structural responses of the impacted SFP slab was performed.

As shown in Figure 5-1, the revised rack drop LS-DYNA model considers the entire SFP slab as well as a portion of the SFP walls directly connected with the slab. Based on SFP design drawings, the SFP is conservatively modeled as a rectangular structure that envelops the actual configuration of the SFP floor. In addition, the impact is conservatively assumed to occur at the center of the SFP floor irrespective of the actual layout of the racks in the SFP. The symmetry in both geometry and loading warrants a quarter drop analysis model. The modeled (13 × 13 cells) rack is conservatively heavier than the heaviest rack (10 × 14 cells) to be installed in the SFP. The effect of stress state on the failure strain of the material is not considered in the rack model, thereby ensuring a conservative damage evaluation of the SFP slab. In addition to the symmetric boundary conditions applied to the two symmetric planes of the quarter model, the top surface nodes of the partially modeled SFP walls are constrained laterally. For additional conservatism, although the SFP is directly founded on grade, the vertical support offered by the underlying soil is not credited in the model; the bottom of the SFP walls (flush with the SFP slab bottom surface) are vertically supported, making the SFP slab effectively an elevated floor. The SFP concrete structure is modeled with solid elements. The reinforcement of the slab is explicitly modeled as a thin shell at each face of the slab with an equivalent thickness. The SFP liner is also modeled as shell elements.

Prior to the rack drop accident, the SFP floor is subjected to the dead load from the water and loaded spent fuel racks in the SFP. Except for the rack drop location, the SFP is conservatively assumed to be occupied by fully loaded racks of spent fuel assemblies. The static loads due to water and loaded racks are applied as pressures to the SFP floor liner. Based on the SFP design, rack layout, and stored fuel weight, the applied pressures are calculated to be 17.55 psi and 20.932 psi, respectively. As the focus of the analysis is the SFP slab, the hydrostatic pressure is not applied to the SFP wall.

Two LS-DYNA simulations are performed for the rack drop analysis. In the first simulation, the SFP floor is loaded only by pressures representing the dead load from the water and the loaded racks. The pressure loads are linearly ramped up in the first 0.01 seconds and remain unchanged during the rest of the 0.5 second simulation. The objective of the first simulation (SFP slab preloading simulation without the dropped rack included in the model) is to determine how much time is needed for the concrete slab to reach the static deflection under the dead load applied incrementally in the

model. Figure 5-2 shows the deformation of the slab at the end of the slab preloading simulation. Figure 5-3 shows the time history of vertical deformation at the center of the slab bottom reinforcement. These results indicate that the bottom of the slab will eventually have a static deformation of about 0.1 inches under the dead load. As shown in Figure 5-3 and Figure 5-4, the vertical deformation is first reached at approximately 0.02 seconds. In the second simulation (the dropped rack included in the model), the SFP floor dead load is applied in the same manner as in the first simulation but the rack is set a few inches above the SFP liner at time zero so the dropped rack will not impact the liner until 0.02 seconds into the simulation when the SFP floor vertical deformation due to the dead load is fully established. In Figure 5-5, the time instant when the dropped rack starts to impact the liner is indicated. The two-step loading of the SFP slab in the rack drop LS-DYNA simulation is also evident in Figure 5-6, which shows the time history of the total load applied to the concrete slab. For conservatism and consistency, no damping effect is considered in either the preloading or the rack drop LS-DYNA simulations. The table below lists the key results of the LS-DYNA rack drop analysis.

Rack Drop Analysis Key Results		**Figure**
Maximum (local) plastic strain of the SFP floor liner	0.0163 in/in	5-7
Maximum stress of the SFP concrete slab bottom reinforcement	9,379 psi	5-8
Maximum (local) stress of the SFP concrete slab top reinforcement	23,967 psi	5-9
Maximum compressive stress of the SFP concrete slab	6,803 psi	5-10

Since the LS-DYNA simulation does not directly account for the thermal loading on the slab, the tensile stress in the bottom reinforcement due to the maximum thru-thickness temperature gradient must be added to the calculated stress from LS-DYNA. Based on a maximum thru-thickness temperature gradient of 122 degrees Fahrenheit (conservatively using abnormal conditions), the induced bending moment in the 10-foot thick slab is 255,000 lbf x in/in and the corresponding tensile stress in the bottom reinforcement is 7,280 psi. Adding this stress to the calculated value from LS-DYNA (9,379 psi), the total combined tensile stress in the bottom reinforcement due to the effects of dead load, thermal load, and the postulated rack drop is 16,659 psi, which is below the design basis yield strength of the steel reinforcement (40,000 psi). Therefore, the displacement of the SFP slab is less than its yield point displacement and the ductility ratio of the SFP slab for this event is less than one. Since ductility ratios less than 1.3 are acceptable per Section 3.5.3 of the BVPS-2 UFSAR, the SFP slab has sufficient capacity to absorb the kinetic energy associated with the postulated rack drop. Thus, the postulated rack drop event does not undermine the global structural integrity of the SFP concrete slab.

From a local standpoint, the postulated rack drop accident results in minor plastic deformation in the SFP floor liner with the maximum plastic strain (0.0163) well below the failure strain of the liner material. From the RAI 17 supplemental response

(page 38), the failure strain for Type 304L stainless steel under biaxial tension is 0.362, which is also applied here to the SFP liner (Type 304). Therefore, there will be no SFP water loss following the rack drop accident. The relatively high concrete compressive stress is only found at the point of impact, indicating minor local damage to the slab concrete.

Finally, when comparing the results from the local rack drop analysis in the RAI 19 supplemental response to the results from the global rack drop analysis, the following observations are made.

i) The rack impact force predicted by the global analysis is approximately 75 percent greater than the impact force from the local analysis due to the fact that the target surface (SFP slab) is stiffer in the global model. The slab is stiffer in the global model because (a) the full thickness (120 inches) of the slab is modeled versus only 24 inches in the local model, and (b) the slab is preloaded by the weight of the water and the spent fuel racks.

ii) Despite its lower impact force, the local analysis predicts higher plastic strains in the SFP liner than in the global analysis. This is because the thickness of the slab in the local model is only one-fifth of the full slab thickness (with an unsupported bottom surface), and therefore the out-of-plane deflection of the slab in the local rack drop analysis is greater than the global analysis result. The out-of-plane deflection of a plate of thickness t is proportional to t^3. The increased deflection compensates for the lower impact force and ultimately leads to higher strains in the SFP liner.

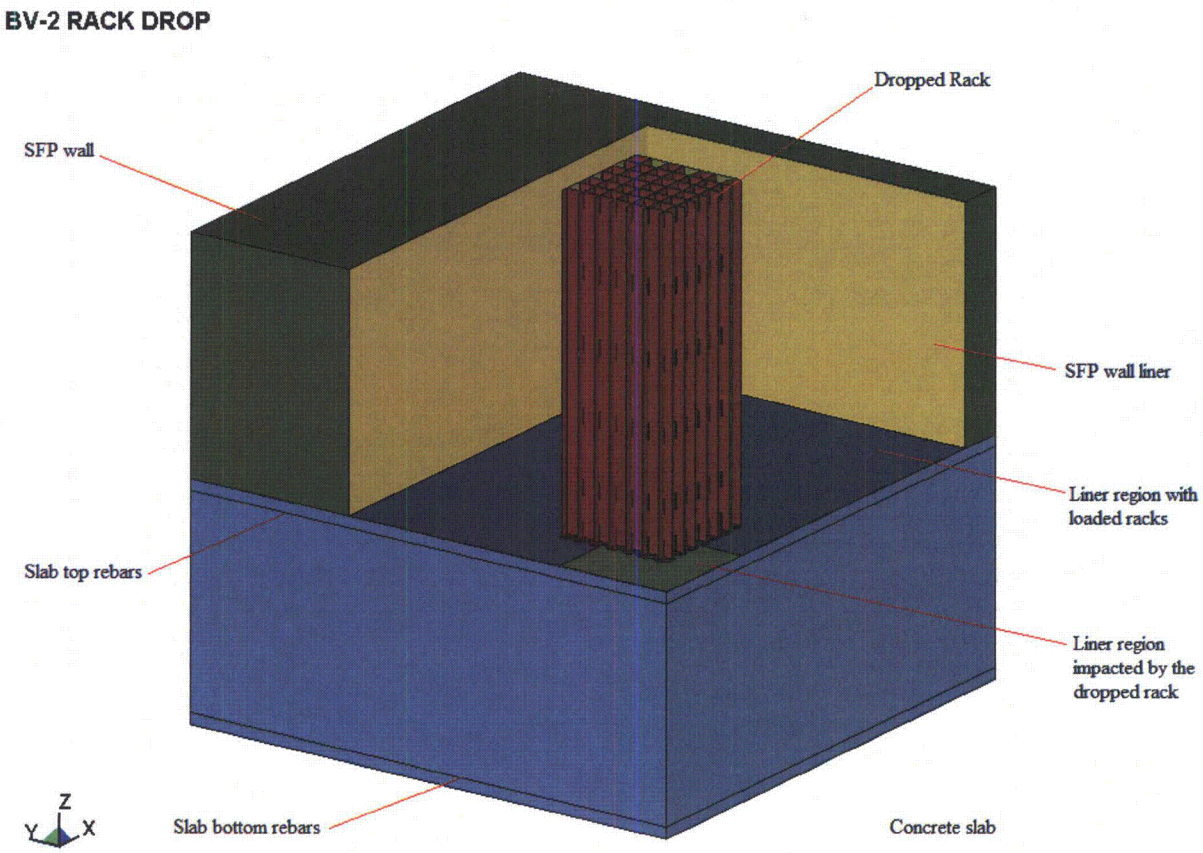

Figure 5-1: Rack Drop LS-DYNA Model

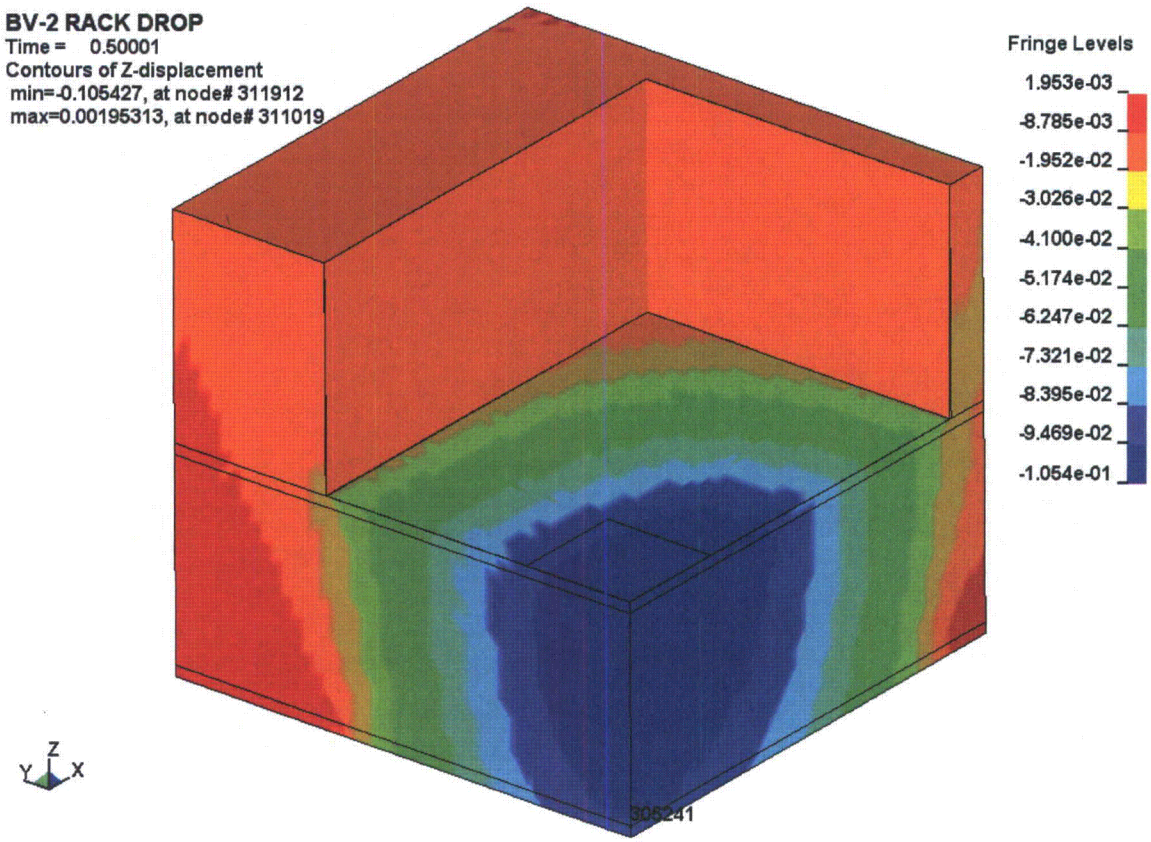

Figure 5-2: SFP Slab Vertical Deformation under Dead Loads from Water and Loaded Racks after 0.5 second simulation Obtained from the Slab Preloading Simulation

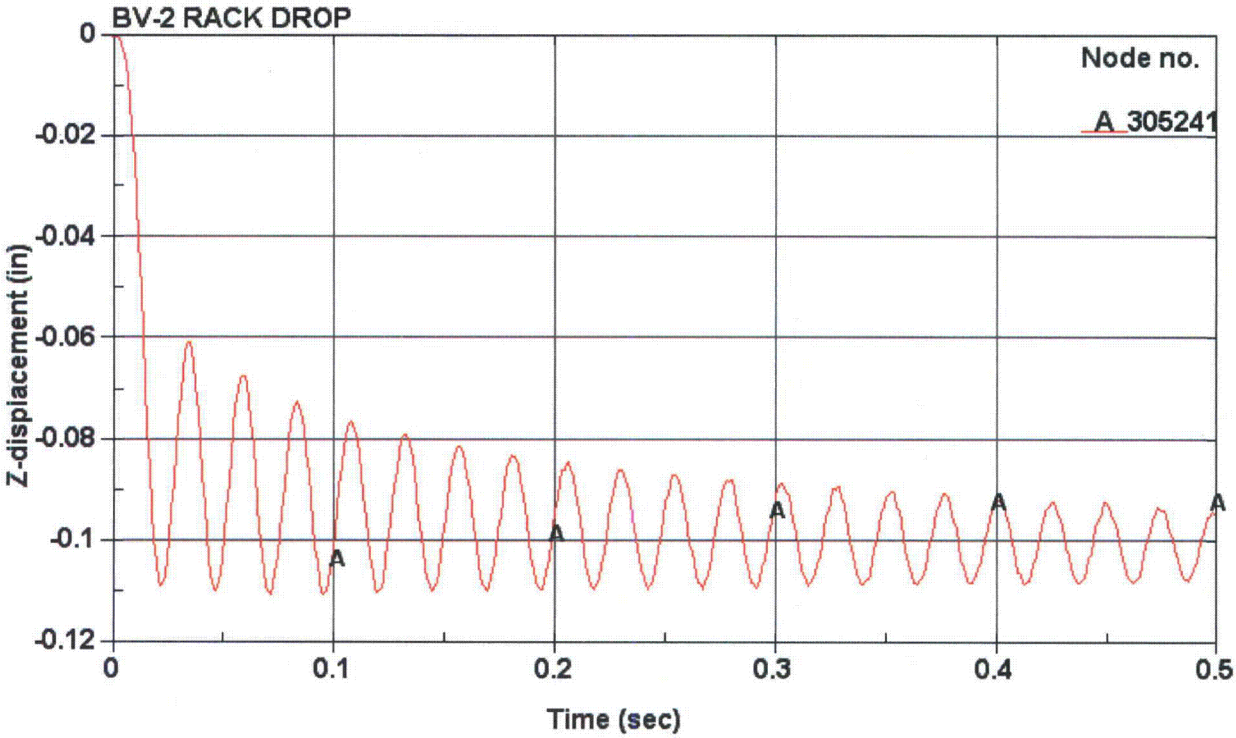

Figure 5-3: Time History of Vertical Deformation at the Center of the Slab Bottom Reinforcement Obtained from the Slab Preloading Simulation

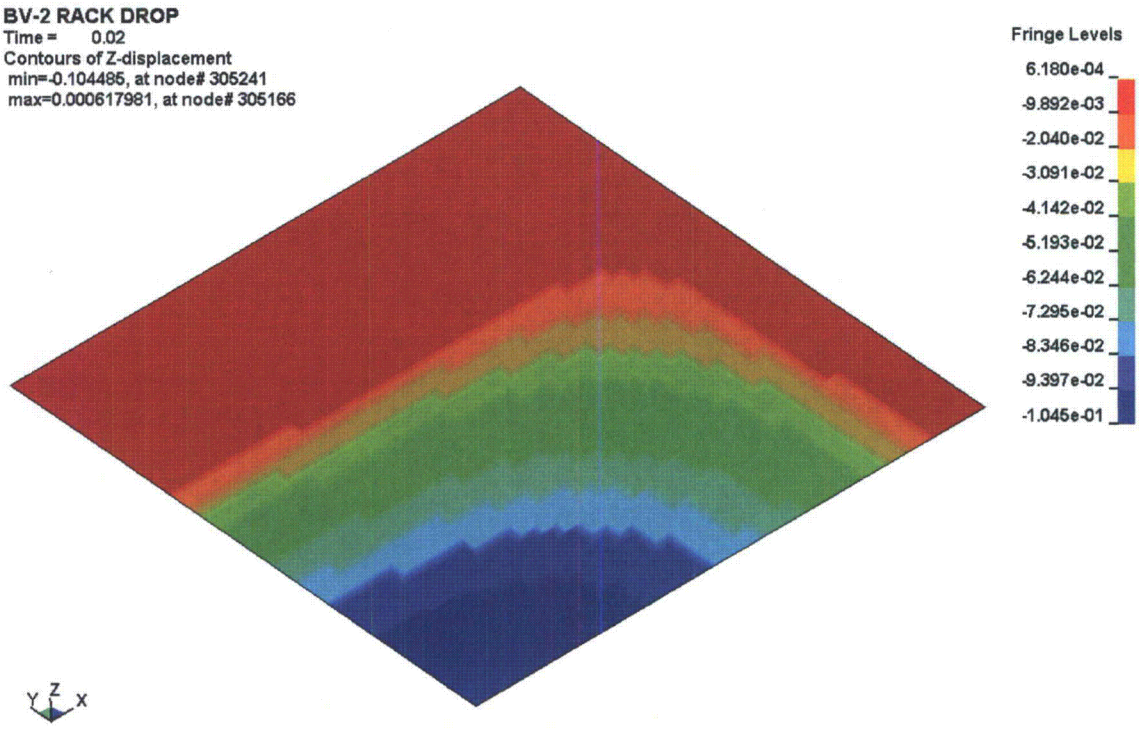

Figure 5-4: Vertical Deformation of the Slab Bottom Reinforcement at 0.02 Second Obtained from the Slab Preloading Simulation

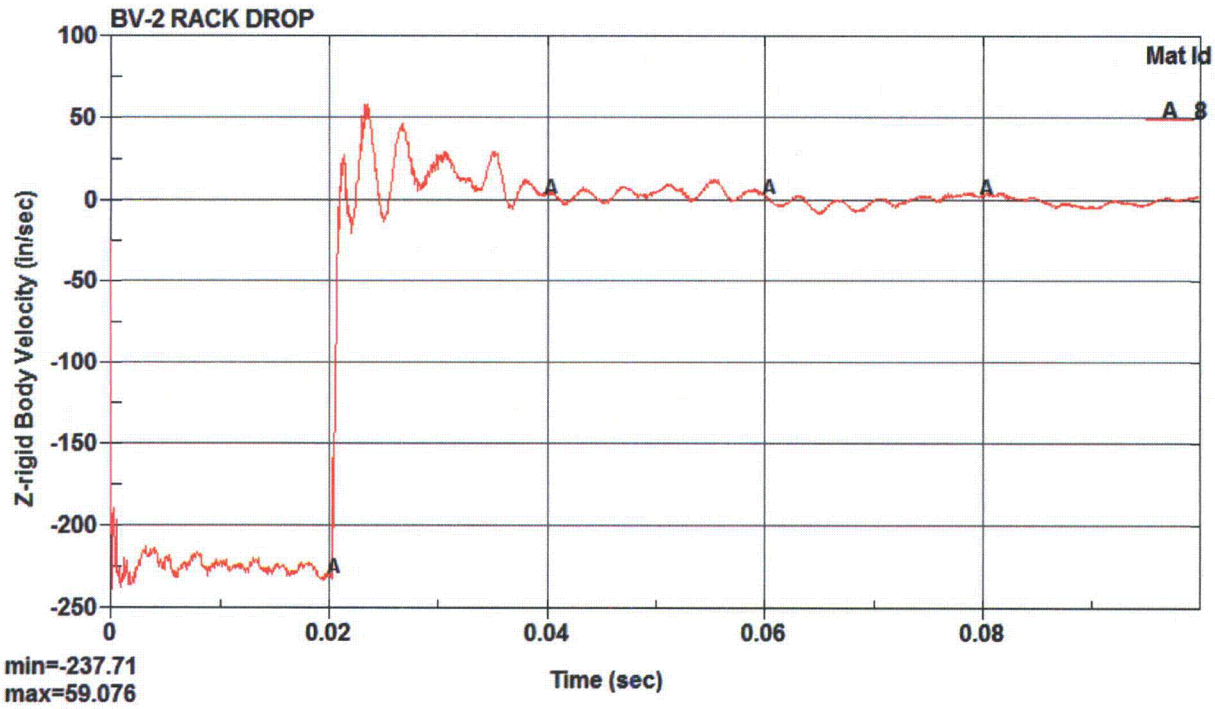

Figure 5-5: Velocity Time History of the Dropped Rack

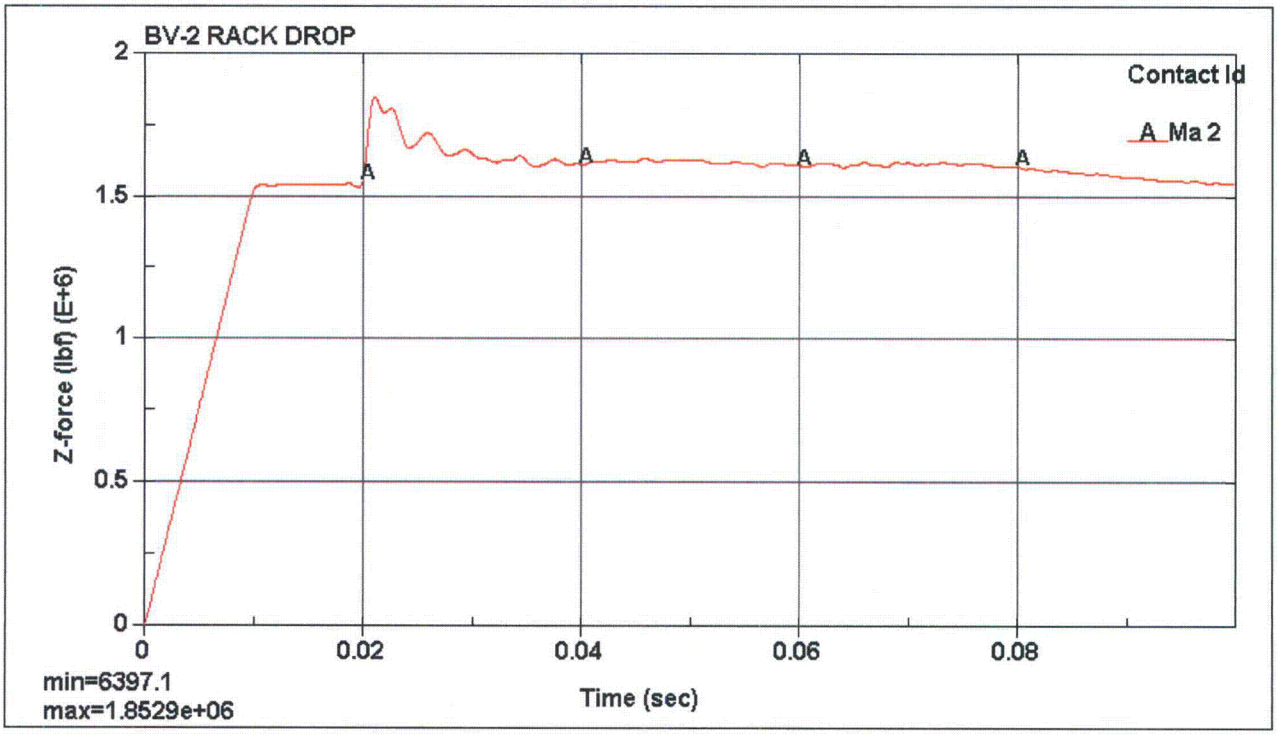

Figure 5-6: Time History of the Total Load Experienced by the SFP Concrete Slab

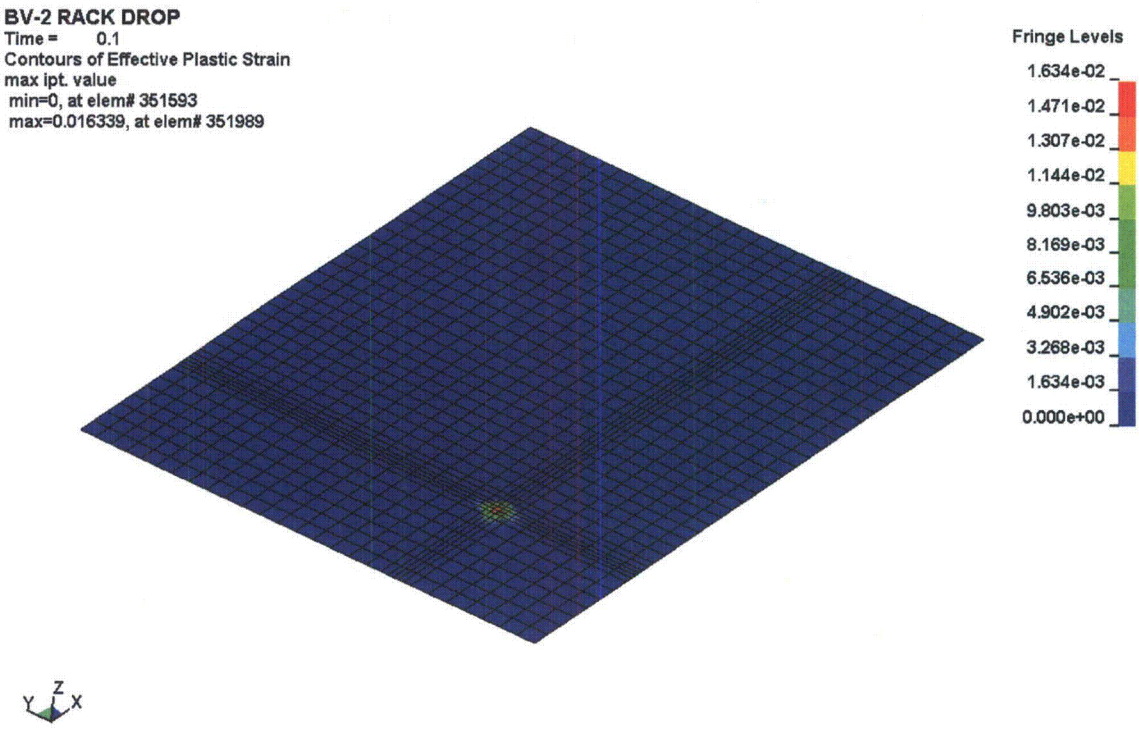

5-7: Maximum Plastic Strain of the SFP Floor Liner after the Rack Drop Accident

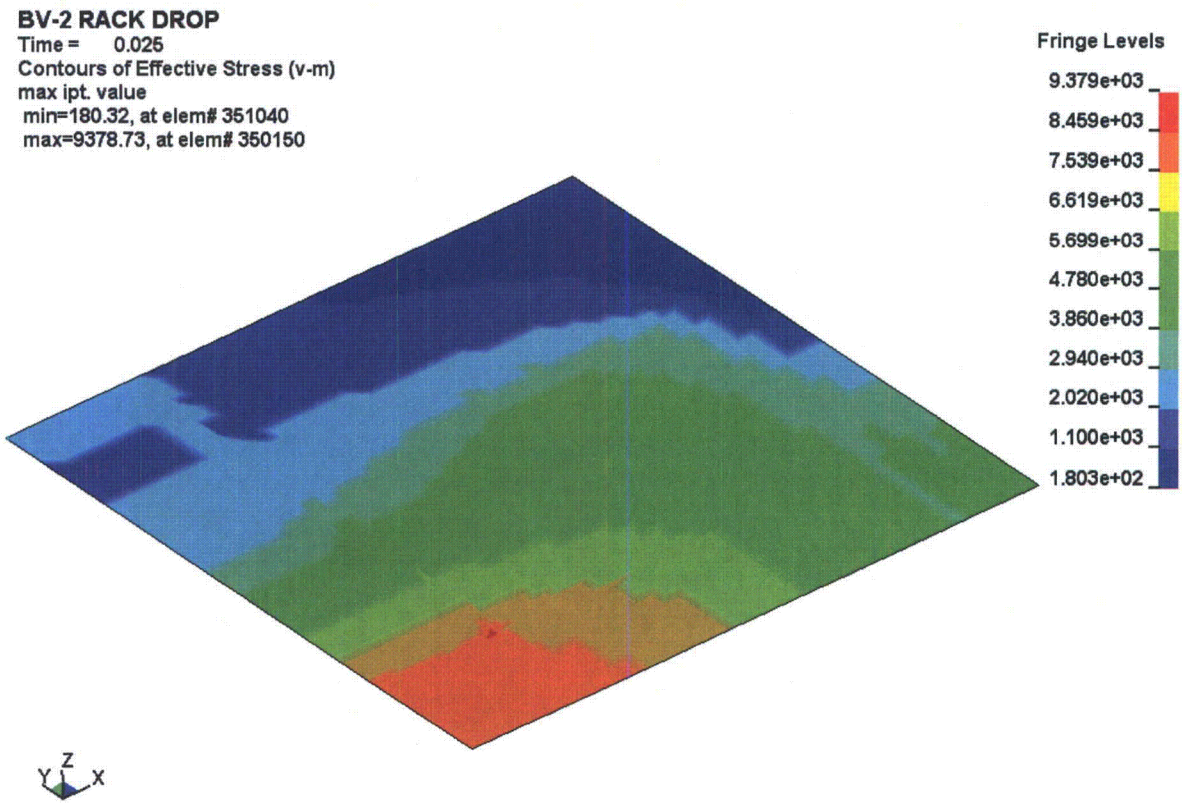

Figure 5-8: Maximum Stress in the Bottom Reinforcement Due to the Rack Drop Accident

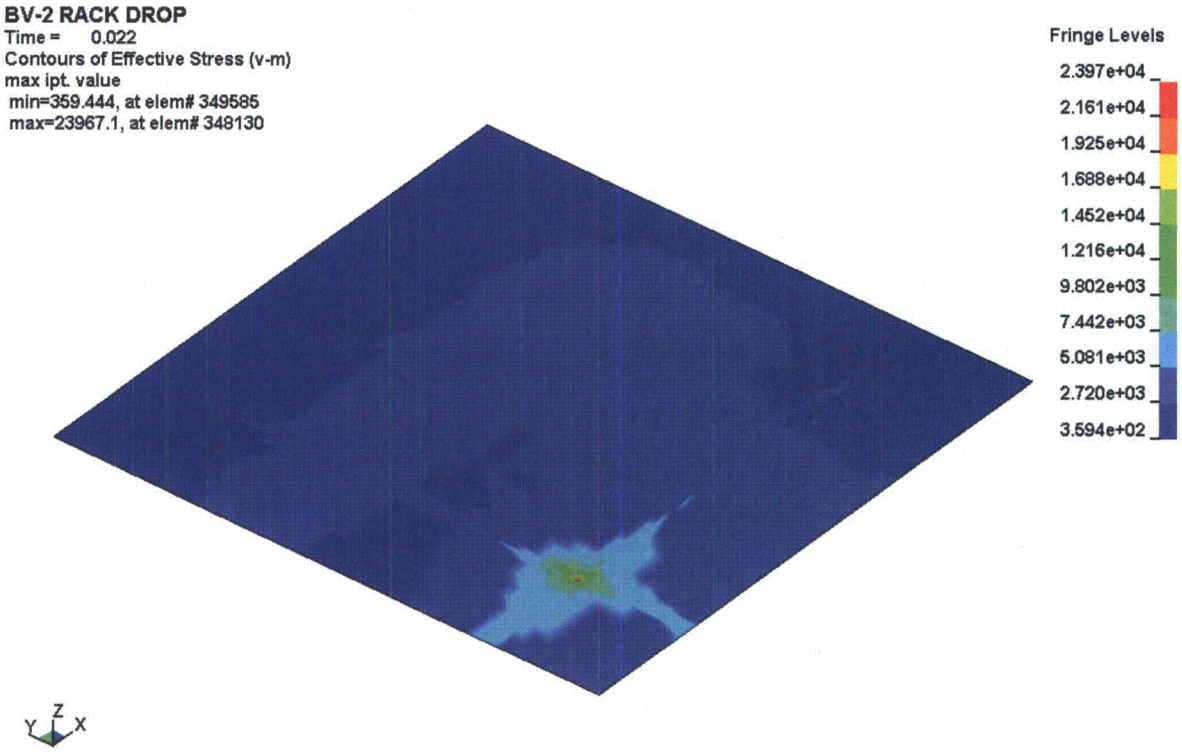

Figure 5-9: Maximum Stress in the Top Reinforcement Due to the Rack Drop Accident

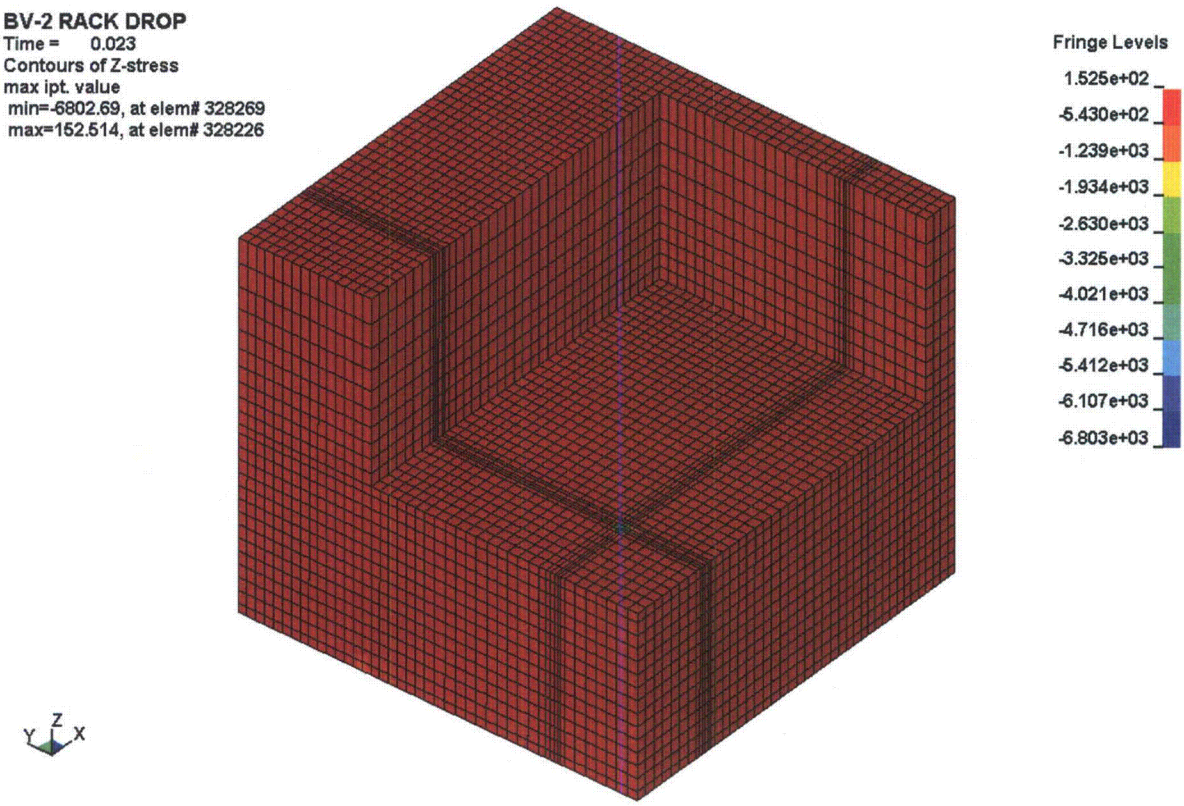

Figure 5-10: Maximum Compressive Stress of the SFP Concrete Slab Resulting Due to the Rack Drop Accident

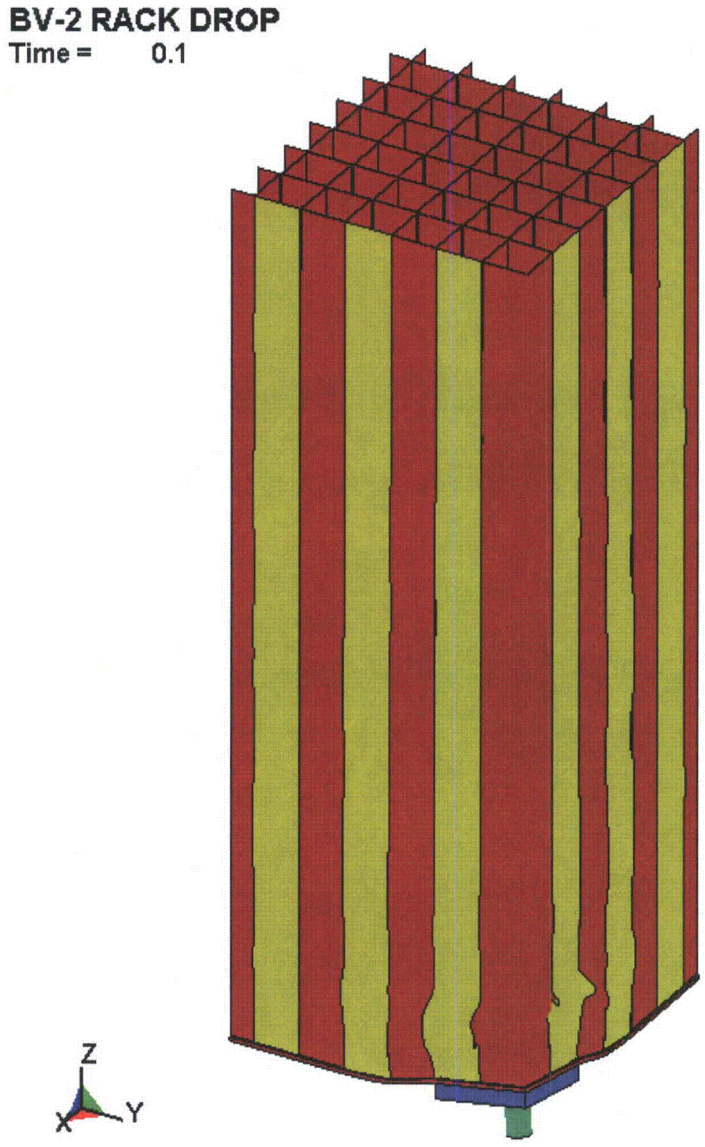

Figure 5-11: Deformed Shape of the Rack Due to the Rack drop Accident

Supplement to RAI-6

1. Appendix D to SRP 3.8.4 states that the structural acceptance criteria are those given in Table 1. OT position paper (GL 78-11) states "When subsection NF, Section III, of the ASME B&PV Code is used for the racks, the structural acceptance criteria are those given in the Table below." The tables in the OT position paper (GL 78-11) and Appendix D to SRP 3.8.4 provide consistent guidance relative to the load combinations and corresponding acceptance limits where seismic and temperature loadings are combined.

The August 9, 2010 supplemental response discusses the shear stresses in the cell-to-cell welds due to the differential thermal growth between neighboring cells. Provide justification that the evaluation described in this response is the enveloping condition for the proposed rack design or provide supplemental information to demonstrate compliance with the guidance defined in Appendix D to SRP 3.8.4 and OT position paper (GL 78-11).

Response:

In the August 9, 2010 supplemental response, it was shown that the shear stress in the cell-to-cell welds resulting from the combined thermal and seismic stresses is less than the most restrictive acceptance limit provided in the 1978 Office of Technology (OT) position paper (Generic Letter 78-11) *Review and Acceptance of Spent Fuel Handling and Storage Applications* for thermal load combinations (that is, 1.5 times normal limits). In order to demonstrate that this is the enveloping condition for the proposed rack design, a three-dimensional finite element model of the largest spent fuel rack has been developed using ANSYS, and the thermal stresses throughout the entire rack have been solved for a bounding temperature distribution. The finite element solution confirms that the highest stressed region coincides with the cell-to-cell welds near the top of the rack where the temperature gradient between neighboring cells is at its maximum (as shown in Figure 6-4).

The ANSYS finite element model used to solve the thermal stress distribution is shown in Figure 6-1. The model accurately reflects the size and dimensions of rack D4, which is the largest of the proposed spent fuel racks for BVPS-2. The support pedestals and rack baseplate are modeled using solid elements. The cell structure, including the cell boxes, filler panels, and corner angles, are modeled using shell elements. Consistent with the rack design drawings, the weld connections are modeled in ANSYS by coupling lines of nodes between adjacent cells, between the baseplate and the cell walls, and between the baseplate and the support pedestals. The bottom surfaces of the support pedestals are fixed in the vertical direction. Finally, a constant coefficient of thermal expansion of 8.9×10^{-6} inch per inch degrees Fahrenheit (in/in-°F) is assigned to all elements in the ANSYS model. This input value conservatively bounds the mean coefficient of thermal expansion for SA-240 304L in going from 70 degrees

Fahrenheit (°F) to 200°F per Section II, Part D of the 1998 American Society of Mechanical Engineers (ASME) Code.

To maximize the temperature gradient across the rack, the thermal stress analysis is performed assuming that half of the rack is loaded with freshly discharged fuel, and the other half is empty. The nodal temperatures applied to each of the cells in the loaded region of the rack are determined from the existing computational fluid dynamics (CFD) analysis of SFP local water temperatures, which is discussed in Section 6.7 of the Licensing Report (Accession No. ML102940458). From the CFD solution, the variation in the SFP water temperature in the vertical direction, inside the hottest cell location, is plotted in Figure 6-2. For the thermal stress analysis using ANSYS, the temperature profile in Figure 6-2 is applied to each storage cell in the loaded region of the rack. Within the empty region of the rack, each node is assigned a temperature of 169.93°F, which is equal to the calculated SFP bulk water temperature following a normal full core offload. The applied temperature of 169.93°F is justified because:

i) The SFP local water temperatures plotted in Figure 6-2 are the result of an abnormal full core offload event (Ta), which means that the temperatures applied to the loaded and empty regions of the rack are operationally consistent. The calculated SFP bulk water temperature for an abnormal full core offload event is 170.33°F. For conservatism, the normal full core offload temperature is applied to the empty region to increase the temperature difference across the rack.

ii) A full core offload event produces the highest temperature levels in the rack, which in turn decreases the mechanical strength properties of the rack material, as well as the allowable stress limits.

The applied temperature distribution for the thermal stress analysis is plotted in Figure 6-3 for the entire rack. The reference temperature used in ANSYS for thermal growth calculations is set to 70°F.

The resulting stress intensity distribution in the rack is plotted in Figure 6-4. The thermal stresses in the rack are negligible everywhere, except the boundary between the loaded and empty regions of the rack. The abrupt change in temperature across this boundary produces shear stresses in the cell-to-cell welds and tensile/compressive stresses in the adjoining cell walls. To determine the maximum shear stress in a single cell-to-cell weld, the nodal reaction forces (in three directions) have been extracted from the ANSYS solution for the topmost row of cell-to-cell welds lying on the boundary plane between the loaded and empty regions of the rack. After post-processing, the maximum resultant force acting on a single cell-to-cell weld is found to be 2,557 pounds of force (lbf); therefore, the maximum shear stress in a single cell-to-cell weld (which is conservatively treated as a 6-inch long, 1/16-inch fillet weld) is 9,644 psi. This stress is less than the weld stress (14,082 psi) originally estimated in Subsection 5.6.10.2 of the Licensing Report (Accession No.

ML091210251) and further discussed in the August 9, 2010 supplemental response. Therefore, the previous supplemental response remains valid relative to the cell-to-cell welds.

As for the cell base metal material, the maximum calculated stress intensity anywhere in the rack structure due to the abnormal thermal load (Ta) is 10,209 psi (as shown in Figure 6-4). Conversely, for the non-thermal loads [that is, D (dead load) + L (live load) + either E (operating basis earthquake [OBE] load) or E' (safe shutdown earthquake [SSE] load)], the maximum stress occurs at the base of the perimeter cells since the cell structure above the base plate acts like a cantilevered beam under horizontal seismic loading. From the DYNARACK simulations, the maximum combined flexure plus tensile/compressive stress due to SSE loading (D + L + E') is 9,381 psi. Notwithstanding the fact that the maximum thermal and seismic stresses occur at opposite ends of the rack, if the two maximums are summed together, the result is 19,590 psi, which is less than the yield strength of SA-240 304L material at 200°F (21,300 psi). Per the January 19, 1979 amendment to the OT position paper, the acceptance limit for load combinations involving thermal loads is the "lesser of 2Sy (yield stress) or Su (ultimate tensile stress) stress range." For SA-240 304L, 2Sy [42.6 thousand pounds per square inch (ksi)] is less than Su (66.2 ksi); therefore, the acceptance limit is 2 x 21,300 psi = 42,600 psi. Since this value is more than two times the maximum combined thermal plus seismic stress (19,590 psi), the calculated stresses in the proposed spent fuel racks for BVPS-2 comply with the acceptance limit provided in the OT position paper (including the January 19, 1979 amendment). The preceding evaluation bounds all load combinations involving thermal loads from the OT position paper since it conservatively combines the seismic stresses due to SSE loading (E') with the thermal stresses due to an abnormal full core offload (Ta), and it compares the result with the acceptance limit for non-faulted conditions (lesser of 2Sy or Su stress range).

Appendix D to the Standard Review Plan (SRP) 3.8.4 invokes the stress limits of the American Society of Mechanical Engineers (ASME) Code, Section III, Subsection NF for Class 3 component supports for spent fuel rack design. In accordance with Subparagraph NF-3121.11, thermal stresses need not be evaluated under Subsection NF. Nevertheless, the maximum combined thermal plus seismic stress of 19,590 psi (which is determined above) is less than faulted condition limit of 1.2Sy (equals 25,560 psi) for combined flexure and axial loads per Subsections NF-3322.1 and F-1334. Under OBE load conditions (D + L + E), the maximum extreme fiber stress at the base of the rack cell structure is 7,195 psi. From Figure 6-4, the thermal stress near the base of the rack due to an abnormal full core offload (Ta) is less than 5,000 psi. Accordingly, the maximum combined thermal plus seismic stress due to OBE is less than 12,195 psi. Therefore, the maximum combined thermal plus seismic stress due to OBE (less than 12,195 psi) is less than the normal (Level A) condition limit for combined flexure and axial loads of 0.6Sy (12,780 psi) per NF-3322.1.

To conclude, the thermal stress analysis performed using ANSYS shows that the enveloping condition for the proposed rack design is the shear stress in the cell-to-cell welds. The maximum shear stress in the cell-to-cell weld, as predicted by ANSYS, is bounded by the previous result given in the August 9, 2010 supplemental response. With regard to the cell base metal, the maximum combined stress in the cell wall remains below the yield strength of the material even when maximum thermal and seismic stresses are summed together irrespective of their locations. This provides a safety factor greater than two when compared against the acceptance limit from the OT position paper (including the January 19, 1979 amendment) for load combinations involving thermal loads. Additionally, as demonstrated above, the maximum combined thermal plus seismic stresses in the rack cell structure are less than the ASME Subsection NF stress limits.

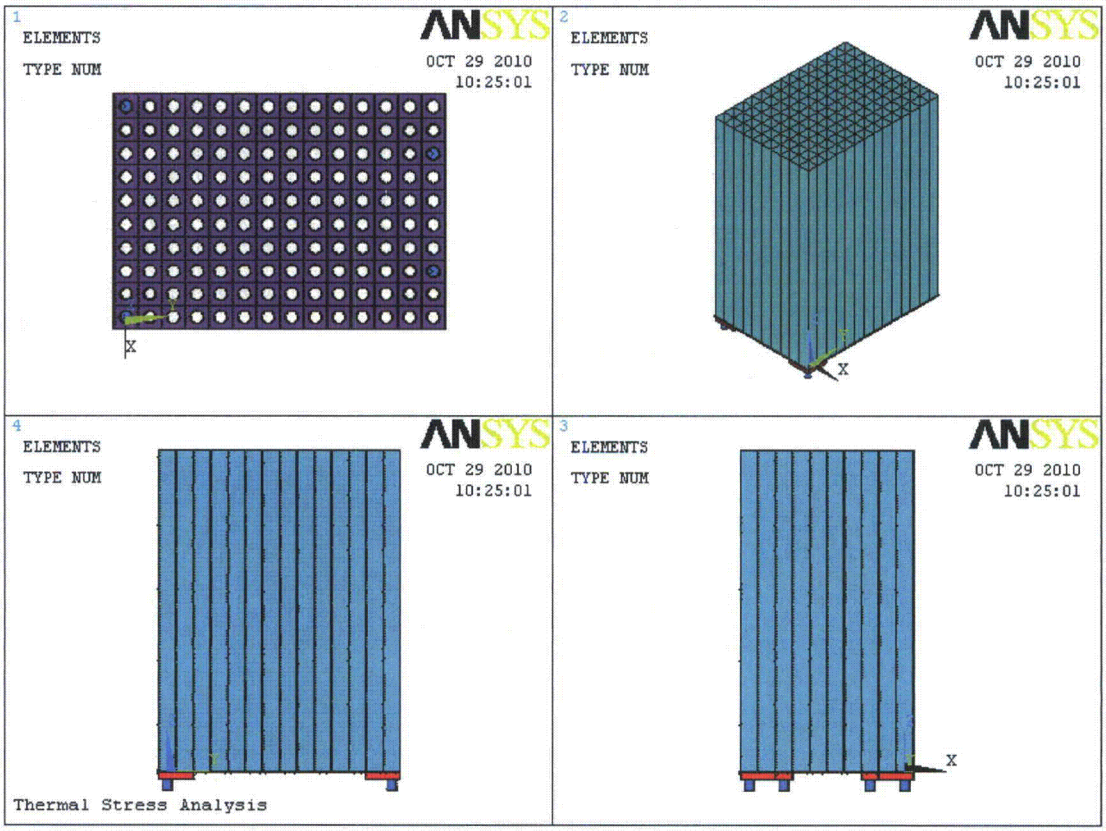

Figure 6-1: ANSYS Finite Element Model of Rack D4

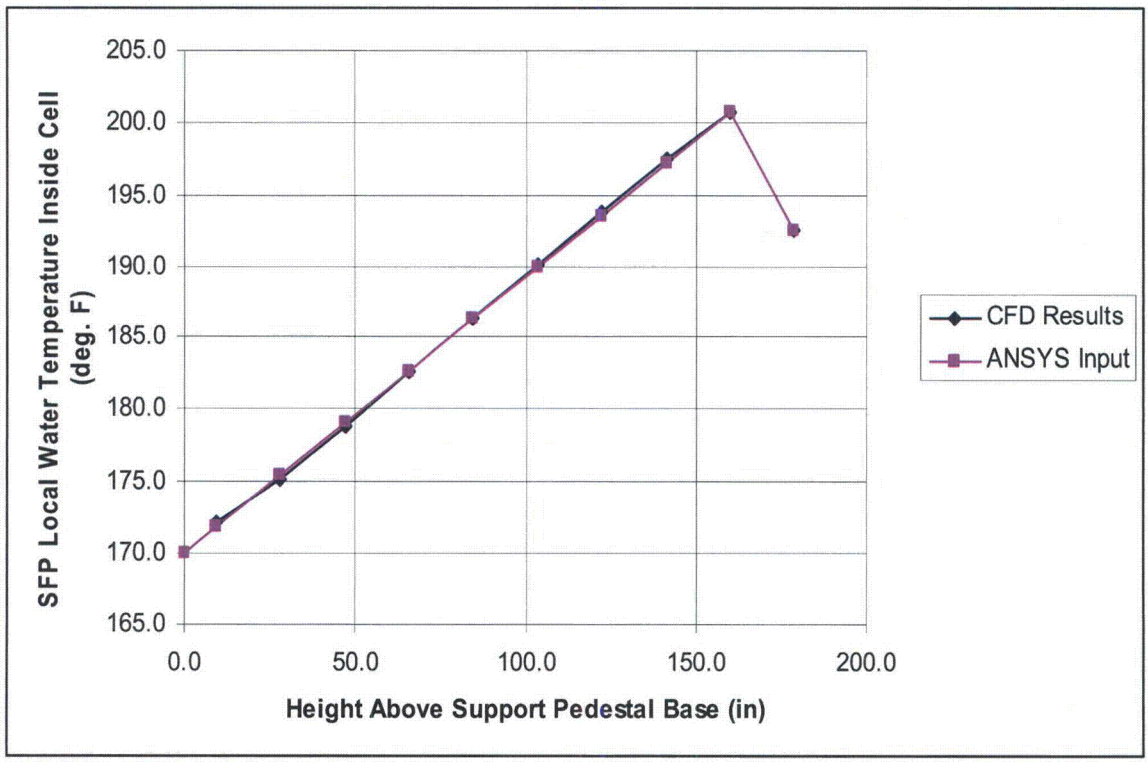

Note: The decrease in water temperature above a height of approximately 160 inches coincides with the upper end point of the active fuel region, which is the primary heat source.

Figure 6-2: SFP Local Water Temperature Inside Hottest Cell Location Due to Abnormal Full Core Offload

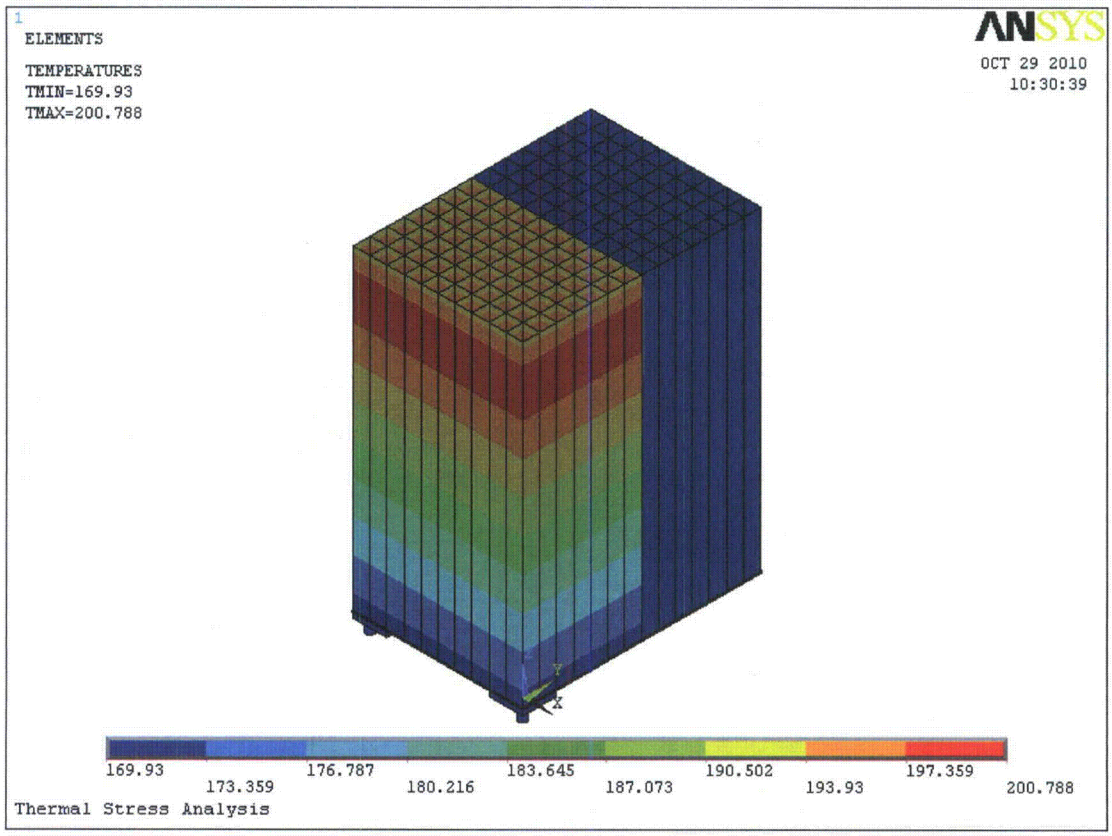

Figure 6-3: Applied Temperature Distribution for Thermal Stress Analysis

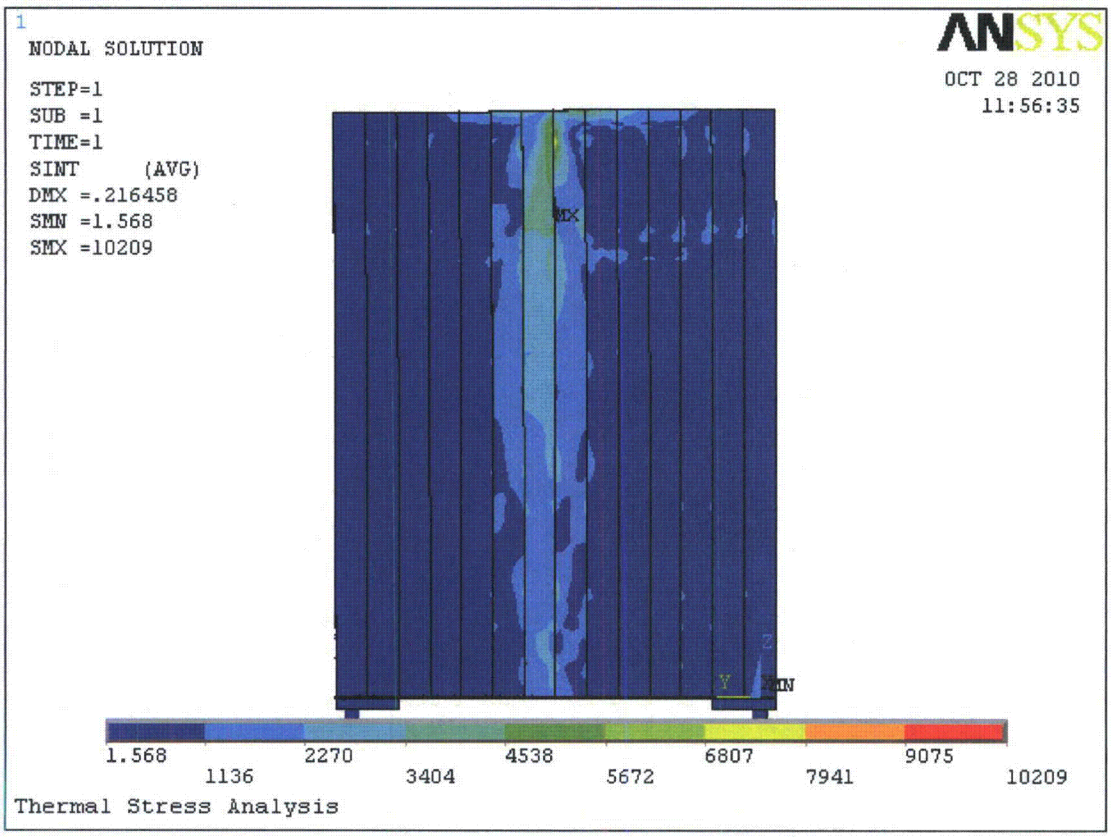

Figure 6-4: Thermal Stresses in the Rack Due to Abnormal Temperature Load (Ta)

Supplement to RAI-8

1. Based on load combinations for concrete structures defined in Section 3.8.3.3 of BVPS-2 UFSAR, Ta should be combined with E' and 1.25E. Load combination (2) in the August 9, 2010 supplemental response includes To (normal condition temperature) rather than Ta (accident condition temperature).

Provide confirmation that appropriate thermal loads, according to the BVPS-2 design basis requirements, have been used in the evaluation of SFP structure.

Response:

UFSAR Section 3.8.3.3 load combinations for concrete structures were simplified due to the absence of live loads, pipe reactions, and postulated pipe breaks, and are summarized as follows:

U = 1.4D + 1.9E	(Based on equation 3.8-3)
U = 1.0D + 1.0Ta + 1.25E	(Based on equation 3.8-8)
U = 1.0D + 1.0Ta + 1.0E'	(Based on equation 3.8-9)
U = 0.75(1.4D + 1.9E + 1.7To)	(Based on equation 3.8-10)

where: U = required section strength
D = dead loads
E = loads generated by the one-half SSE (OBE), where E = ½ E'
E' = loads generated by the SSE
To = normal thermal loads, where To = Ta for this evaluation
Ta = abnormal thermal loads

For this evaluation Equation 3.8-8 is bounded by Equation 3.8-9 since OBE is equal to one-half of SSE (E = ½ E'), therefore, the load combination 1.0D + 1.0Ta + 1.25E is not explicitly analyzed. For the SFP structural evaluation, Ta is conservatively substituted for To in Equation 3.8-10.

Finally, the thru-thickness temperature gradients that comprise the thermal load Ta for the SFP structure have also been reviewed to confirm that they are consistent with the BVPS-2 design basis, particularly the ambient temperatures surrounding the SFP structure. As a result of this assessment, the calculated temperature gradients through the SFP walls and the slab have been revised. In some cases (for example, the SFP North Wall, SFP Slab) the thru-thickness temperature gradients have increased due to the use of a lower ambient temperature on the outside face of the concrete (opposite to the SFP water). In other cases (for example, the SFP East Wall), the thru-thickness temperature gradients have decreased due to the fact that the cask loading area and the transfer canal are flooded with water during a full core offload event. The following table summarizes the thru-thickness temperature gradients used in the previous analysis for the thermal load Ta and those used in the updated analysis.

SFP Component	Thru-Thickness Temperature Gradient, ΔºF	
	Previous Analysis	Updated Analysis
West Wall	95.5	86.8
North Wall	93.3	140.1
South Wall	93.6	87.8
East Wall	99.5	63.3
East-South Wall	97.6	59.9
South-East Wall	96.8	58.3
Slab	94.8	121.5

2. The August 9, 2010 supplemental response does not discuss the capacity reduction factor (Phi factor). Please confirm that appropriate Phi factors have been considered for two-way and one-way shear evaluations.

Response:

Per Section 9.2.1.3 of ACI 318-71, a capacity reduction factor, ϕ, equal to 0.85 was used in both the one-way and the two-way shear evaluations discussed in the August 9, 2010 supplemental response.

3. Provide further justification that the tributary area methodology used in one-way shear evaluation is conservative.

Response:

To validate the tributary area methodology and quantify the degree of conservatism associated with the one-way shear evaluation, a simple finite element model of the SFP east wall (which is limiting based on the one-way shear evaluation presented in the August 9, 2010 supplemental response) has been created in ANSYS and analyzed for two different pressure load cases. The finite element model resultant shear forces on the wall are then compared with the results obtained using the tributary area methodology. The following paragraphs describe the ANSYS model, the load cases analyzed, and the results.

The finite element model, shown in Figure 8-1, is comprised entirely of shell elements. The height, width, and thickness of the SFP East Wall are modeled in ANSYS as 486 inches, 263.5 inches, and 24 inches, respectively. Consistent with the one-way shear evaluation, the top edge of the wall is assumed to be free and the other three edges are fixed. In the first load case, a uniform pressure of 15.93 psi (which equals the total out-of-plane load on the SFP east wall due to the load combination 1.4D + 1.9E) is applied over the entire face of the wall, and the nodal reaction forces are summed along each of the three fixed edges to determine the shear force distribution. The following table compares the calculated shear forces on the fixed edges of the wall as obtained from ANSYS and from the tributary area method.

East Wall Edge Boundary	ANSYS Finite Element Method		Tributary Area Method	
	Shear Force (lbf)	Percentage of Total Applied Load (%)	Shear Force (lbf)	Percentage of Total Applied Load (%)
Left	881,840	43.23	881,902	43.22
Right	881,834	43.23	881,902	43.22
Bottom	276,338	13.55	276,562	13.55

The ANSYS results and the results obtained using the tributary area method show excellent agreement confirming that the tributary area method (as presented in the August 9, 2010 supplemental response) is a valid method for distributing a uniformly distributed (out-of-plane) load on a wall to its support edges.

In the second load case, a linear varying pressure load is applied to the same model to reflect the precise loading on the SFP east wall due to the load combination 1.4D + 1.9E (which are the limiting SFP wall and load combination from the one-way shear evaluation). In other words, instead of applying a uniform pressure of 15.93 psi over the entire wall, a linear varying pressure is applied to the wall, which has a minimum value of 3.99 psi at the top edge of the wall and a maximum value of 28.24 psi at the bottom edge of the wall (as shown in Figure 8-2). The following table compares the calculated shear forces on the fixed edges of the wall as obtained from ANSYS versus the one-way shear forces evaluated for the August 9, 2010 supplemental response, which are estimated using the tributary area method.

East Wall Edge Boundary	ANSYS Finite Element Method		Shear Force Evaluated for August 9, 2010 Supplemental Response (lbf)	Percentage Difference Between Results (%)
	Shear Force (lbf)	Percentage of Total Applied Load (%)		
Left	809,955	39.25	881,902	+8.88
Right	809,946	39.25	881,902	+8.88
Bottom	443,892	21.51	446,947	+0.69

The above table shows that the one-way shear forces evaluated for the August 9, 2010 supplemental response for the SFP east wall are slightly conservative as compared to the more precise finite element solution. In particular, the one-way shear force on the left and right edges of the SFP east wall are overestimated by more than 8 percent due to the fact that the tributary area method, as implemented, assumes a uniformly distributed load on the wall and conservatively ignores the fact that the actual load is biased towards the bottom edge. Conversely, the calculated shear force on the bottom edge of the SFP East Wall in the August 9, 2010 supplemental response does account for the linear varying pressure load, therefore, the level of conservatism is reduced.

The tributary area methodology has been validated against an independent finite element solution, and it is shown to be capable of accurately predicting the shear forces on the support edges of a uniformly loaded wall. Furthermore, the tributary area methodology, as implemented for the one-way shear evaluation of the BVPS-2 SFP structure, yields conservative results for the vertical support edges. The results presented above are based on the SFP east wall. All SFP walls are rectangular and have three fixed edges. The tributary area method and finite element solution vary only by the wall dimensions. Therefore, the conclusions from the SFP east wall evaluation are valid for all SFP walls.

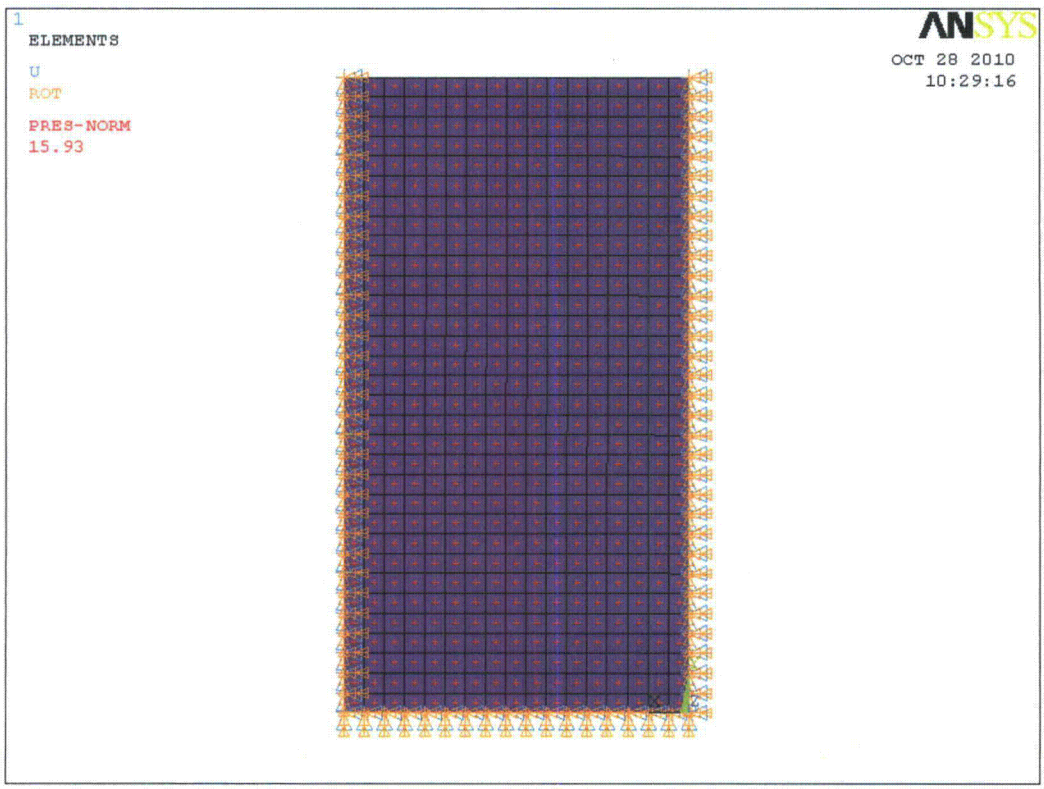

Figure 8-1: ANSYS Finite Element Model of SFP East Wall Under Uniformly Distributed Pressure Load

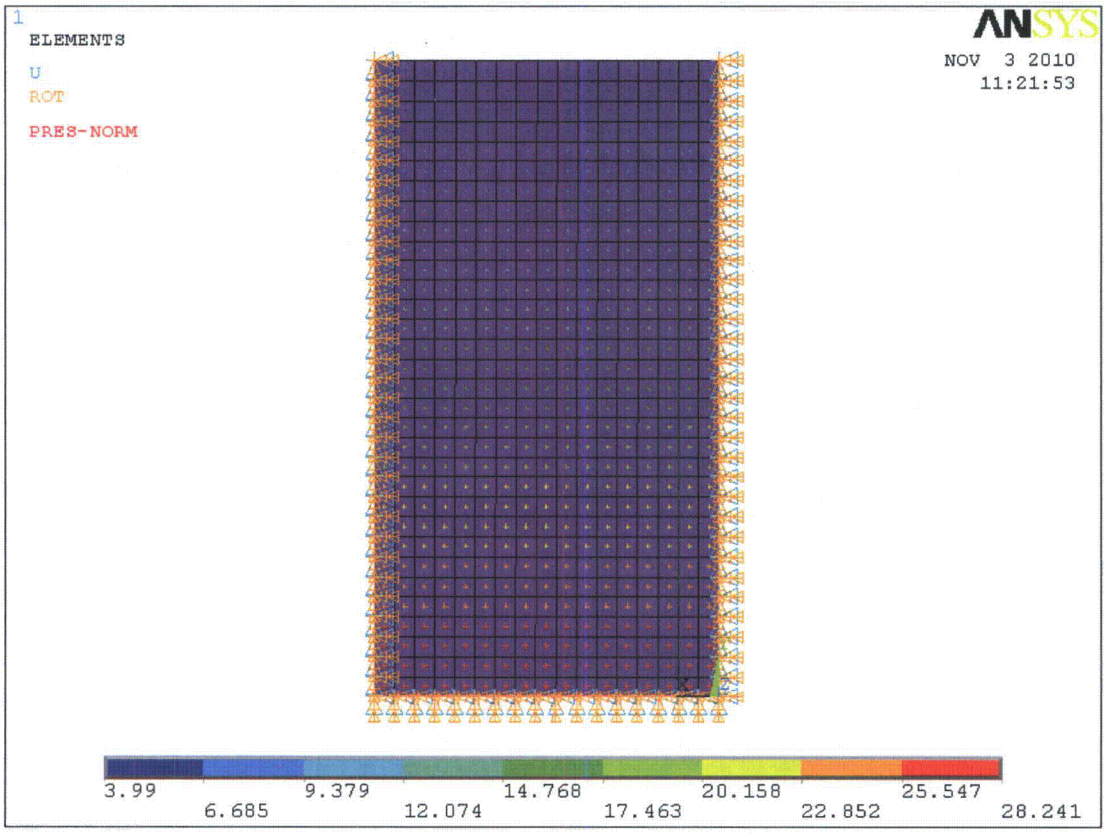

Figure 8-2: ANSYS Finite Element Model of SFP East Wall Under Linear Varying Pressure Load

4. The August 9, 2010 supplemental response states that the liner plate is not analyzed because it is designated as seismic category II. However, according to Section 3.2.1.2 of BVPS-2 UFSAR, a seismic category II classification is identified as those SSCs whose failure could adversely affect safety-related, seismic category I components. Therefore, the response does not adequately address the effects of SFP temperature rise on the liner plate integrity.

Response:

The Unit 2 spent fuel pool liner consists of 1/4-inch plate with vertical stiffeners spaced every 18 inches on center. The stiffeners consist of structural T-shapes welded to the liner plate. The T-shapes anchor the liner to the concrete. Welded headed studs were not used to anchor the liner plate to the concrete.

At the time the Unit 2 spent fuel pool was designed and constructed, no existing code governed the design of spent fuel pool liners. It was elected to use design criteria from ASME, Section III, Division 1 - 1974 Edition, Nuclear Plant Components, Subsection

NA with Addenda up to Summer 1976 as applicable, for the design of the spent fuel pool liner.

Based on the design basis calculations for the SFP liner, the liner design used the maximum differential temperature from the postulated thermal conditions for the SFP. The bounding thermal condition was based on the boiling temperature of the pool at the site elevation. The other thermal conditions have a smaller differential temperature and yield lower stress values. Therefore the existing design basis calculation for the SFP liner bounds the thermal loads for the SFP re-rack and the safety factors for the liner are not impacted.

With regard to the rack drop analysis, the original design basis for the SFP liner did not consider an accidental drop of a spent fuel rack since the racks were installed in the pool prior to plant start-up. ASME Section III, Division 1 is a stress-based code which is best suited for load limited events. Since the rack drop accident is an energy limited event, a strain based criteria has been used to evaluate the structural integrity of the SFP liner due to the impact. Specifically the maximum calculated strain in the SFP liner is compared against the true fracture strain limit for 304 stainless steel.

5. The August 9, 2010 supplemental response states: "The shear safety factors reported above are not adversely affected by the temperature rise in the pool since thermal loads tend to cause compression in the SFP slab and wall cross sections, which has a positive (increasing) effect on shear capacity." Contrary to this statement, the temperature rise tends to expand the SFP liner and since the liner is anchored to the concrete, the liner expansion will induce a tensile load on the wall.

Provide further information that the effects of the SFP liner heat-up has been included in the evaluation of the SFP concrete structure according to the BVPS-2 design basis requirements.

Response:

The structural evaluation of the BVPS-2 SFP concrete structure has been revised to include the effects of the SFP liner heat-up. As noted by the NRC staff, the thermal expansion of the SFP liner will induce tensile loads in the walls since the liner is anchored to the concrete. The tensile load per unit width, F, induced in each SFP wall or slab due to SFP liner heat-up is determined based on the following formula:

$$F = \frac{\alpha_s \Delta T_s - \alpha_c \Delta T_c}{\left(\frac{1}{E_s t_s} + \frac{1}{E_c t_c} \right)}$$

where α_s = coefficient of thermal expansion of Type 304 stainless steel (= 8.79 × 10^{-6} in/in-Δ°F);

α_c = coefficient of thermal expansion of concrete (= 5.5 × 10^{-6} in/in-Δ°F);

ΔT_s = temperature rise of SFP liner (Table 8-1);

ΔT_c = temperature rise of concrete (Table 8-1);

E_s = elastic modulus of Type 304 stainless steel (= 27.6 × 10^6 psi);

E_c = elastic modulus of concrete (psi) = $57{,}000\sqrt{f_c'}$;

t_s = thickness of SFP liner (= 0.25 in);

t_c = thickness of concrete wall (Table 8-1);

For all SFP components except for the east-south and south-east Walls, the temperature rise of the SFP liner (ΔT_s) is taken as 100.3°F, which is the difference between the SFP bulk water temperature following an abnormal full core offload (170.3°F) and the stress-free temperature at the time of construction (which is assumed to be 70°F). The east-south and south-east Walls, which separate the SFP from the transfer canal, are not governed by the abnormal full core offload condition. This is because during an offload the transfer canal is in communication with the SFP, and as a result the water temperature on both sides of the walls is roughly equal. The thermal gradients and the induced tensile loads in the east-south and south-east Walls are greatest during normal operating conditions when the transfer canal is drained. Thus, the tensile forces in the SFP walls and slab, as summarized in Table 8-1, are the limiting results from either the abnormal thermal condition (Ta) or the normal operating thermal condition (To). Furthermore, the limiting results in Table 8-1 are conservatively used for all load combinations involving thermal loads, regardless of whether the load combination specifies To or Ta.

Table 8-1: Induced Tensile Loads in SFP Walls and Slab Due to SFP Liner Heat-Up

SFP Component	Concrete Wall Thickness, t_c (in)	Temperature Rise of SFP Liner, ΔT_s (Δ°F)	Temperature Rise of Concrete, ΔT_c (Δ°F)	Tensile Load per Unit Width, F (lbf/in)
West	72	100.3	56.0	3,840
North	90	100.3	24.6	5,026
South	88	100.3	52.7	3,983
East	24	100.3	70.4	3,124
East-South	54	85.3	55.3	2,954
South-East	48	85.3	56.2	2,907
Slab	120	100.3	33.5	4,725

Note: For each SFP component, the temperature rise of the concrete (ΔT_c) is equal to the difference between the mean (thru-thickness) temperature of wall/slab and the stress-free temperature (which is assumed to be 70°F).

The tensile loads summarized in Table 8-1 have been included in the one-way and two-way shear stress evaluations and the bending moment evaluation for the SFP walls for the load combinations involving thermal loads (To, Ta). Specifically, for the one-way and two-way shear stress evaluations, the permissible shear stress carried by the concrete has been computed for each SFP wall according to the interaction formula given in Section 11.4.4 of ACI 318-71 and the tensile loads in Table 8-1 (including the appropriate ACI load factors). Likewise, the bending moment capacities of the SFP walls have been adjusted according to the axial force-moment interaction diagrams for those walls. The results of the one-way and two-way shear stress evaluations are summarized in Tables 8-2 and 8-3, respectively. The results of the bending moment evaluation are summarized in Table 8-4. All calculated safety factors are greater than 1.0.

Table 8-2: Results of One-Way Shear Evaluation

SFP Wall/Edge	Load Combination	Permissible Shear Stress, v_c (psi)	Calculated Shear Stress, v_u (psi)	Safety Factor
North/Vertical	1.4D + 1.9E	93.11	39.64	2.35
	D + Ta + E'	82.72	32.63	2.54
	0.75(1.4D + 1.9E + 1.7To)	79.86	29.73	2.69
North/Bottom	1.4D + 1.9E	93.11	52.40	1.78
	D + Ta + E'	82.72	43.14	1.92
	0.75(1.4D + 1.9E + 1.7To)	79.86	39.30	2.03
South/Vertical	1.4D + 1.9E	93.11	28.62	3.25
	D + Ta + E'	84.68	23.55	3.60
	0.75(1.4D + 1.9E + 1.7To)	82.36	21.46	3.84
South/Bottom	1.4D + 1.9E	93.11	33.96	2.74
	D + Ta + E'	84.68	27.95	3.03
	0.75(1.4D + 1.9E + 1.7To)	82.36	25.47	3.23
West/Vertical	1.4D + 1.9E	93.11	60.45	1.54
	D + Ta + E'	78.44	49.32	1.59
	0.75(1.4D + 1.9E + 1.7To)	74.40	45.34	1.64
West/Bottom	1.4D + 1.9E	93.11	73.91	1.26
	D + Ta + E'	78.44	60.29	1.30
	0.75(1.4D + 1.9E + 1.7To)	74.40	55.44	1.34
East/Vertical	1.4D + 1.9E	93.11	79.25	1.17
	D + Ta + E'	68.87	62.82	1.10
	0.75(1.4D + 1.9E + 1.7To)	62.20	59.44	1.05
East/Bottom	1.4D + 1.9E	93.11	70.94	1.31
	D + Ta + E'	68.87	54.20	1.27
	0.75(1.4D + 1.9E + 1.7To)	62.20	53.20	1.17

Table 8-2 (continued): Results of One-Way Shear Evaluation

Notes:

1) To is conservatively assumed to equal Ta. Therefore, the load combination 0.75(1.4D + 1.9E + 1.7To) bounds D + Ta + 1.25E.
2) In the absence of any axial load, the nominal permissible shear stress is 93.11 psi (= $2\phi_v\sqrt{f_c'}$).
3) The entire SFP West Wall is conservatively assumed to be 48 inches thick for the one-way shear stress evaluation even though the lower portion of the wall is actually 72 inches thick.
4) For SFP East Wall, the one-way shear stress along each edge is calculated at a distance d (where d is defined as distance from extreme compression fiber to centroid of tension reinforcement) from the face of the intersecting wall/slab as permitted by Section 11.2.2 of ACI 318-71.
5) The SFP slab is 10-feet thick and founded on grade; therefore, a shear failure of the SFP slab is not limiting. This is evident from the May 3, 2010 RAI response, which shows that the slab has a safety factor greater than 13 (without taking credit for the subgrade) against punching shear failure due to the rack drop event.

Table 8-3: Results of Two-Way Shear Evaluation

SFP Wall	Load Combination	Permissible Shear Stress, u_c (psi)	Calculated Shear Stress, u_u (psi)	Safety Factor
North	1.4D + 1.9E	186.23	30.00	6.21
	D + Ta + E'	165.44	24.70	6.70
	0.75(1.4D + 1.9E + 1.7To)	159.73	22.50	7.10
South	1.4D + 1.9E	186.23	19.82	9.40
	D + Ta + E'	169.35	16.31	10.39
	0.75(1.4D + 1.9E + 1.7To)	164.71	14.86	11.08
West	1.4D + 1.9E	186.23	48.71	3.82
	D + Ta + E'	156.88	39.73	3.95
	0.75(1.4D + 1.9E + 1.7To)	148.81	36.53	4.07
East	1.4D + 1.9E	186.23	84.47	2.20
	D + Ta + E'	137.73	66.95	2.06
	0.75(1.4D + 1.9E + 1.7To)	124.40	63.36	1.96

Note: For all SFP walls, the two-way shear stress is calculated at a distance d/2 from the perimeter edge (where d is defined as distance from extreme compression fiber to centroid of tension reinforcement) as permitted by Section 11.10.2 of ACI 318-71.

Table 8-4: Limiting Results of Bending Moment Evaluation

SFP Component /Limiting Direction	Governing Load Combination	Interaction Moment Capacity, M_c (lbf-in/in)	Moment Load, M_u (lbf-in/in)	Safety Factor
North/Horizontal	0.75(1.4D + 1.9E + 1.7To)	1.56×10^6	8.72×10^5	1.79
South/Horizontal	0.75(1.4D + 1.9E + 1.7To)	7.09×10^5	5.41×10^5	1.31
West (Bottom Section)/Vertical	1.4D + 1.9E	7.18×10^5	5.84×10^5	1.23
East/Horizontal	0.75(1.4D + 1.9E + 1.7To)	7.49×10^4	4.18×10^4	1.79
East-South/ Horizontal	0.75(1.4D + 1.9E + 1.7To)	1.90×10^5	1.57×10^5	1.21
South-East/ Horizontal	0.75(1.4D + 1.9E + 1.7To)	1.68×10^5	1.55×10^5	1.08
Slab	0.75(1.4D + 1.9E + 1.7To)	1.24×10^6	9.76×10^5	1.27

Notes:

1) To is conservatively assumed to equal Ta.
2) The minimum safety factor for the SFP west wall is associated with the bottom section of the wall, which is controlled by bending in the vertical direction. At this location, the vertical bending moments due to thermal loads (To or Ta) are in the opposite direction to the vertical bending moments due to dead load (D). Hence, the SFP West Wall is governed by the load combination 1.4D + 1.9E. The other SFP walls are controlled by bending in the horizontal direction, where the bending moments due to the thermal load and dead load are additive. Therefore, they are governed by the load combination 0.75(1.4D + 1.9E + 1.7To).

Supplement to RAI-17

1. Using the Hancock-MacKenzie model to determine failure strain is not acceptable (triaxial factor of 0.6065). The triaxial factor needs to be 0.5 based on more recent models (As discussed during the public meeting, the NRC documented its acceptance of a minimum triaxiality factor of 2.0 for cases of biaxial tension in the safety evaluation report (SER) written for Amendment 7 to the Certificate of Compliance (CoC) for the Holtec International (HI)-STORM 100 cask system (located in ADAMS at ML093620075).

Response:

The shallow drop analysis has been re-performed in LS-DYNA using a constant triaxial factor of 0.5. More precisely, the failure strain limits for the base metal and weld material are input in LS-DYNA as 0.5 times the corresponding 98 percent exceedance uniaxial failure strain, and they remain constant throughout the simulation. The response to Question 2 details the material model and summarizes the results.

2. Document the basis for using the INL paper for determining the strain rate amplification curve for the weld material. Additionally, the supplemental information will document the discussion regarding RAI 17 to provide explicit details regarding the material model curve which was used in the LS-DYNA analysis. This will include information relative to where the strain rate amplification was applied (i.e., only the stress was increased) and where the triaxiality factor was applied to provide a clear understanding of what the value for the true failure is for the shallow-drop accident analysis. Coupled with this discussion, justification regarding the strain amplification value(s) used and at what point during the analysis these values are used will be provided. This justification should focus on how the amplification factor is applied to the true stress-strain curve in the LS-DYNA model, i.e. describing whether an iterative procedure is used in LS-DYNA to capture the strain rate value and then apply the corresponding amplification factor or whether a constant strain rate amplification factor is applied to the true stress-strain curve.

Response:

In the previous analysis, the Idaho National Laboratory *Impact Testing of Stainless Steel Material at Room and Elevated Temeratures* (INL) paper was used to determine the strain rate amplification curve for the weld material based on the similar chemical compositions of SA-240 304L base metal and Type 308 weld material. The shallow drop analysis has been re-performed using the strain rate amplification data from the INL paper for the base metal material only. No strain rate amplification factors are applied to the weld material. The following paragraph describes the material model curves for the base metal and the weld material in more detail, including the precise

manner in which the triaxiality factor and the strain rate amplification factors are applied to the material model curves.

The base metal material (SA-240 304L) and the weld material (Type 308) are both modeled in LS-DYNA using material model MAT_024 (MAT_PIECEWISE_LINEAR_PLASTICITY). The true stress-strain curves are input as user-defined curves where the data points in the plastic deformation region are determined according to the following power law relationship:

$$\sigma = K\varepsilon^n$$

where σ = true stress
K = strength coefficient
ε = true strain
n = strain-hardening exponent

The methodology used to obtain the values of K and n, for a specific material, from a set of engineering stress-strain data (for example, strength properties from ASME Section II, Part D) is provided in Holtec Position Paper DS-307, *Construction of True-Stress-True-Strain Curve for LS-DYNA Simulations*, Revision 2 (submitted to the NRC under Docket 72-1032 for the HI-STORM FW License Application). Table 17-1 provides the values of K and n that are used to model the behavior of the base metal material and the weld material in the shallow drop analysis for the BVPS-2 spent fuel racks. The yield strength, ultimate strength and Young's Modulus of the weld material are conservatively assumed to be identical to those of the base material, leading to an identical power law relationship for both materials (values of K and n) as shown in Table 17-1.

Table 17-1

VALUES OF K AND n

Material Type	Reference Temperature (°F)	K (psi)	n
Base Metal (SA-240 304L)	150	1.21×10^5	0.235
Weld Metal (Type 308)	150	1.21×10^5	0.235

The ultimate failure strain limits for the base metal material and the weld material are determined by multiplying the 98 percent exceedance uniaxial failure strains (0.724 and 0.493 for the base metal and weld material, respectively) by a triaxial factor of 0.5 (for biaxial tension). The resulting failure strain limits for the base metal material and the weld material are 0.362 and 0.2465, respectively, which are input to LS-DYNA as constant value properties.

The strain rate amplification curve applied to the base metal material, which is based on the INL paper, is shown in Figure 17-1. Throughout the simulation, the strain rate amplification factor for each base metal element is determined based on the instantaneous strain rate of the element (that is, an iterative procedure is used). The time-dependent and element-dependent amplification factors are applied only to the stress values in the true stress-strain curve for the base metal material.

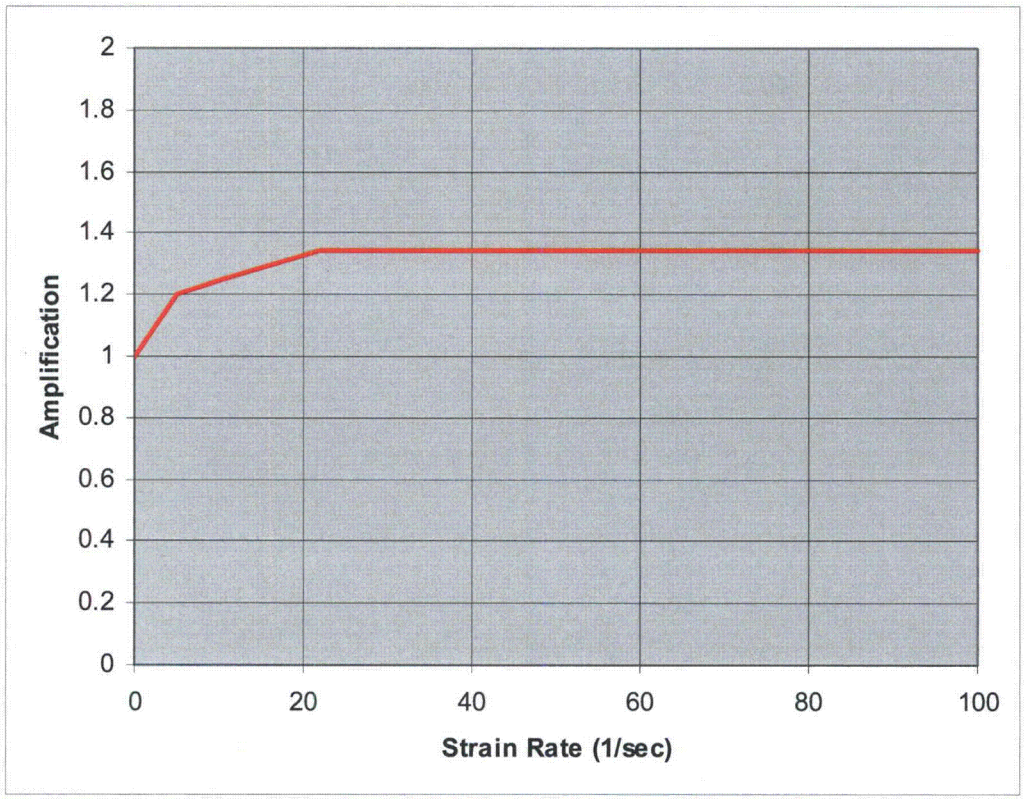

Figure 17-1: Strain Rate Amplification Curve for Base Metal Material

In conjunction with the change in triaxial factor and the elimination of strain rate effects for the weld material, the finite element model of the impacted rack has been updated to include the 1/4" thick x 10" deep reinforcement bar, which is welded to the exterior cell walls of the rack (above the neutron sheathing) around the entire rack perimeter. The previous shallow drop analysis conservatively ignored the presence of the reinforcement bar. Since the reinforcement bar reinforces only the perimeter cell walls, the shallow drop analysis has been expanded to consider two drop locations:

i) a vertical fuel assembly drop from a height of 24 inches above the rack onto a perimeter cell wall;
ii) a vertical fuel assembly drop from a height of 24 inches above the rack onto an interior cell wall.

The results for the fuel assembly drop onto a perimeter cell are shown in Figures 17-2 through 17-4, and summarized in Table 17-2. The results for the fuel assembly drop onto an interior cell are shown in Figures 17-5 through 17-7, and summarized in Table 17-3.

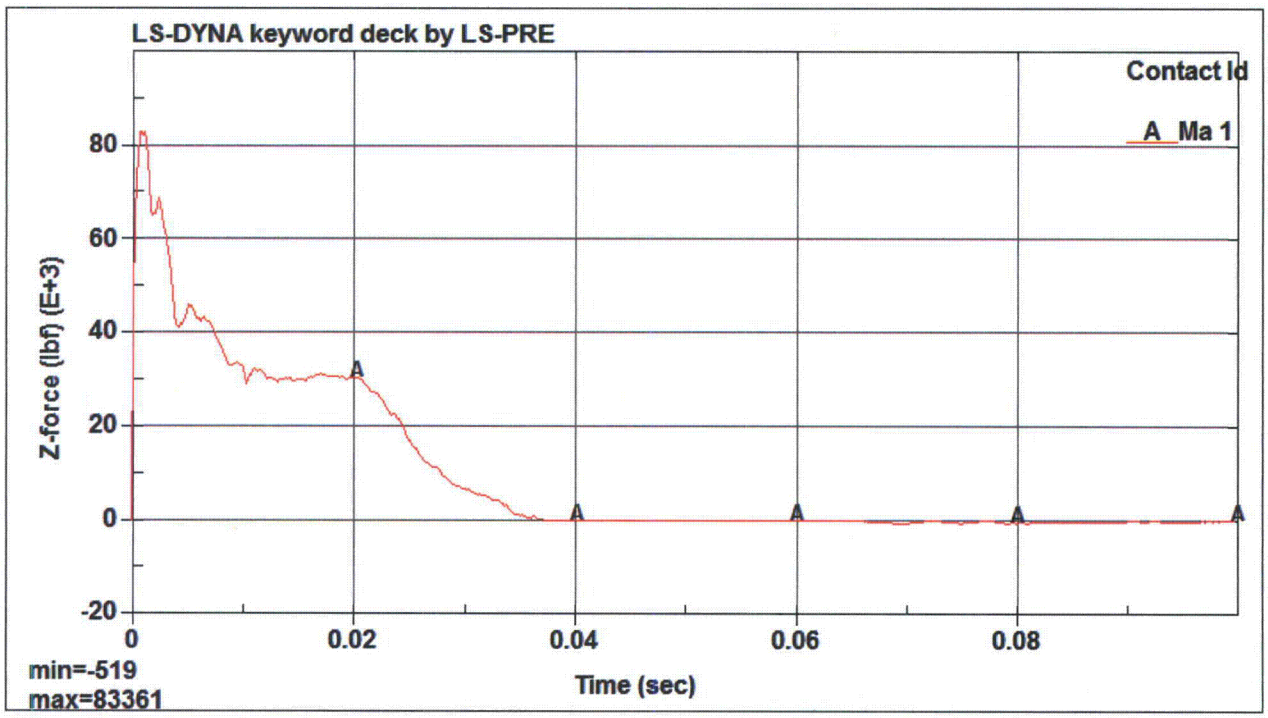

Figure 17-2: Impact Force Time History for Drop onto a Perimeter Cell

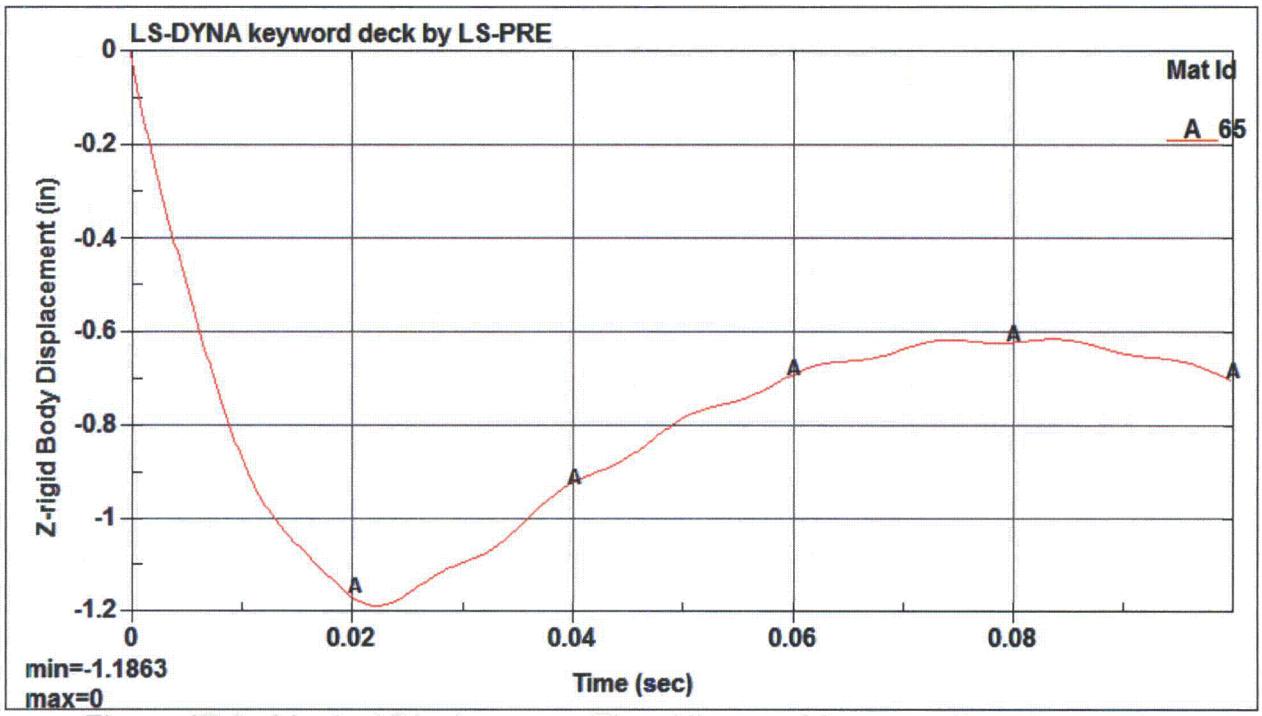

Figure 17-3: Vertical Displacement Time History of Dropped Fuel Assembly for Perimeter Cell Impact

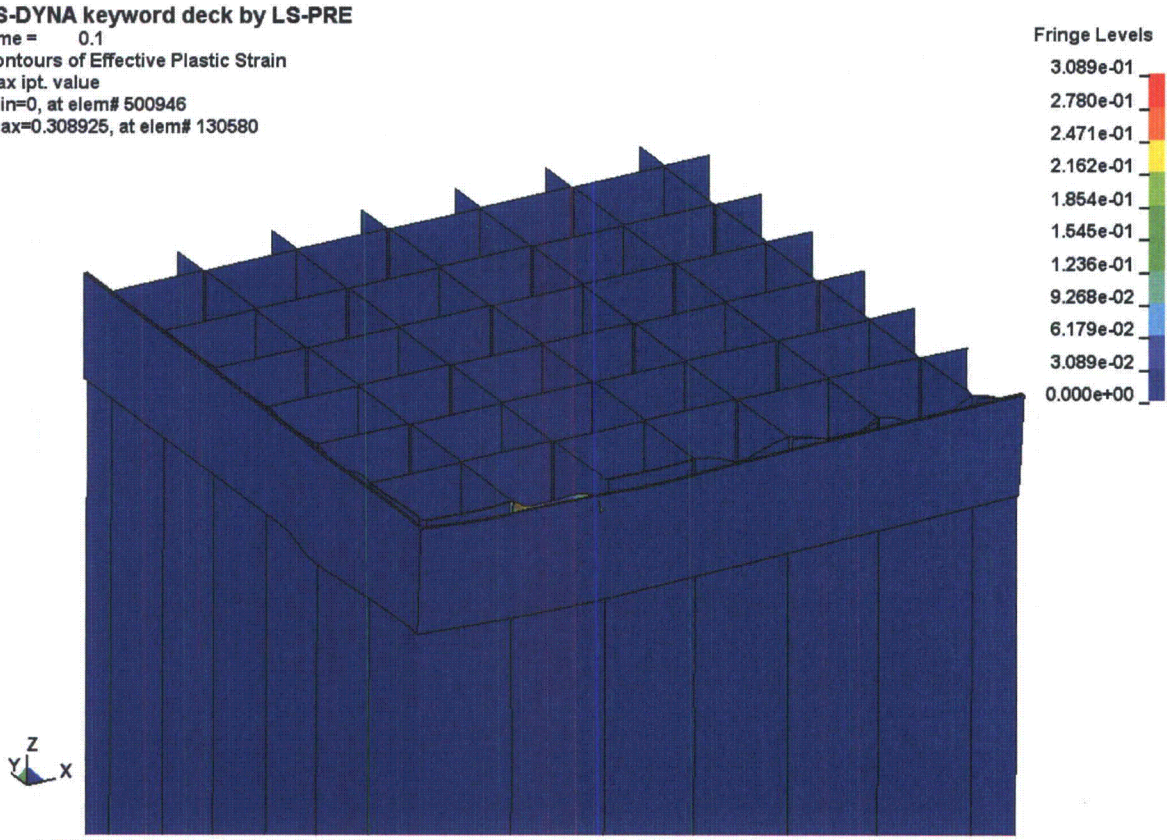

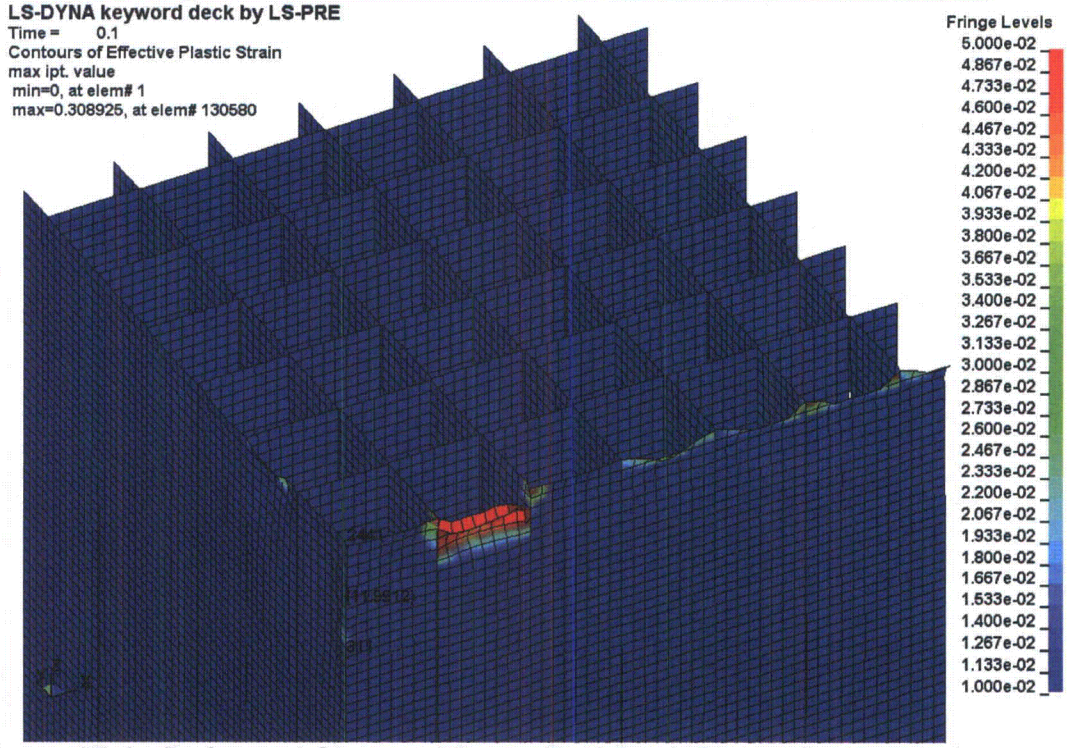

Figure 17-4: Deformed Shape of Spent Fuel Rack Due to Perimeter Cell Impact

Table 17-2 RESULTS FOR FUEL ASSEMBLY DROP ONTO PERIMETER CELL	
Impact Duration (sec)	0.0375
Peak Impact Force (lbf)	83,361
Fuel Assembly Vertical Displacement (in)	1.2
Plastic Deformation Measured from the Rack Top (in)	12.0

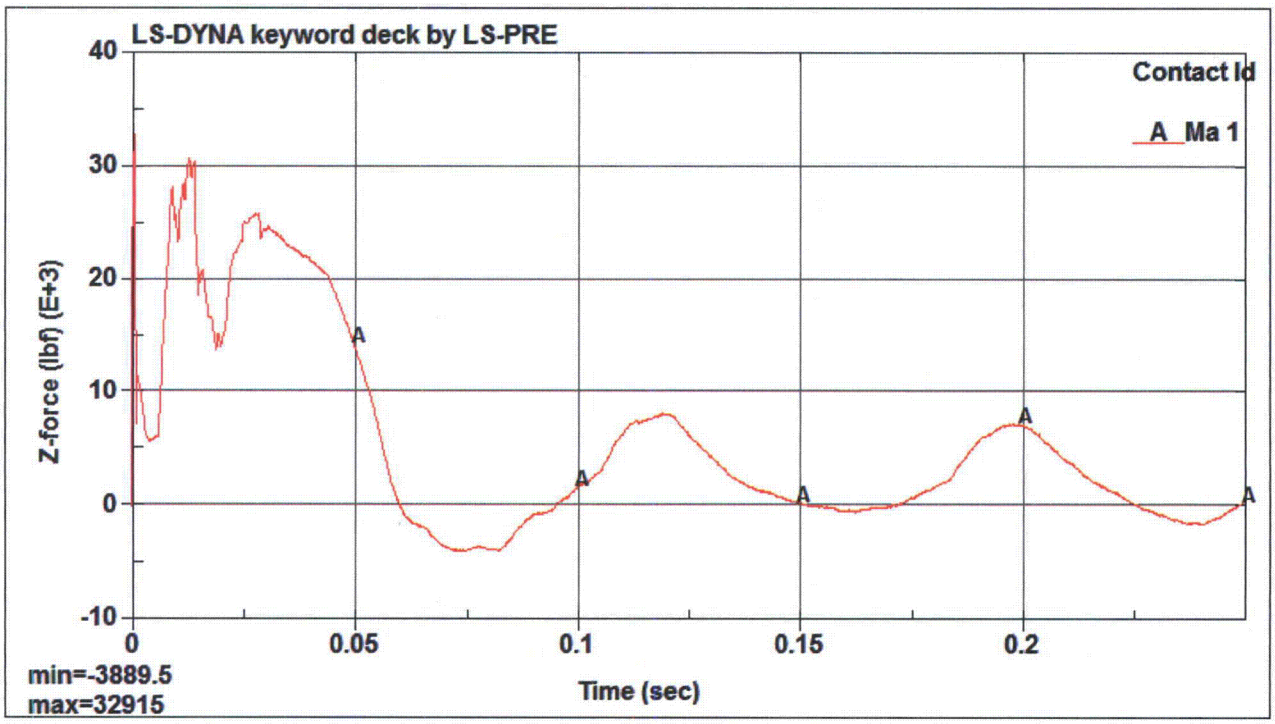

Figure 17-5: Impact Force Time History for Drop onto an Interior Cell

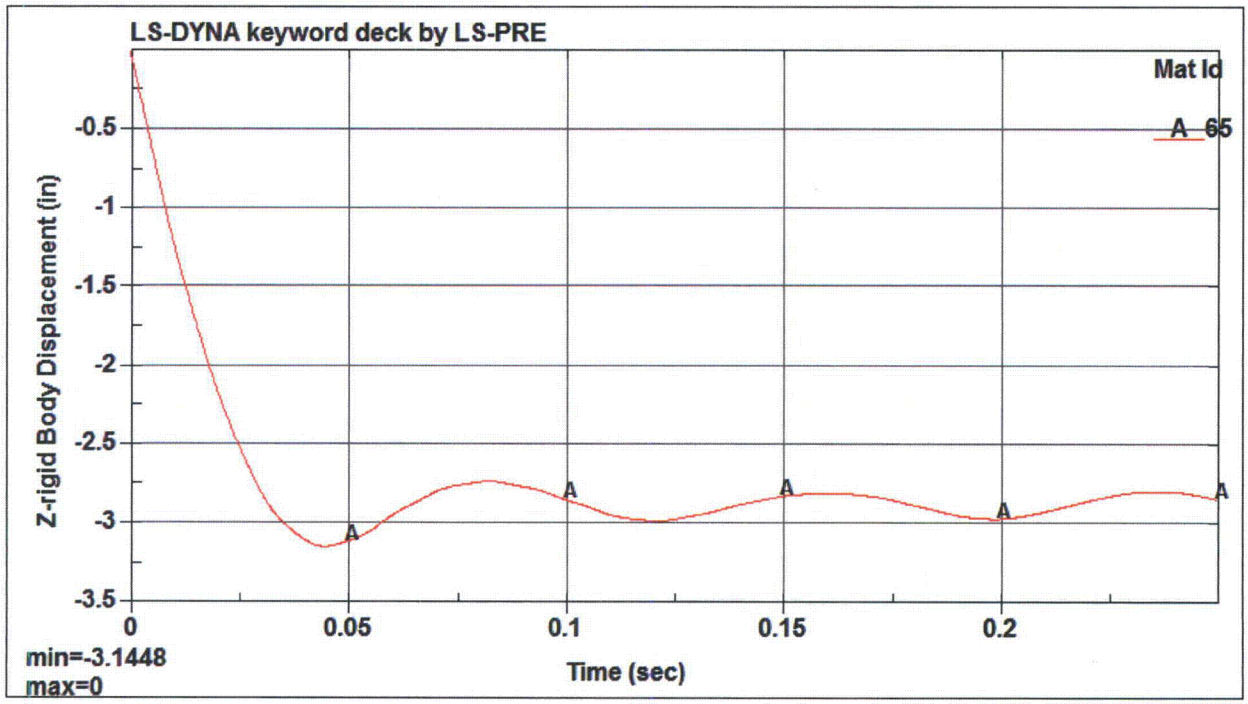

Figure 17-6: Vertical Displacement Time History of Dropped Fuel Assembly for Interior Cell Impact

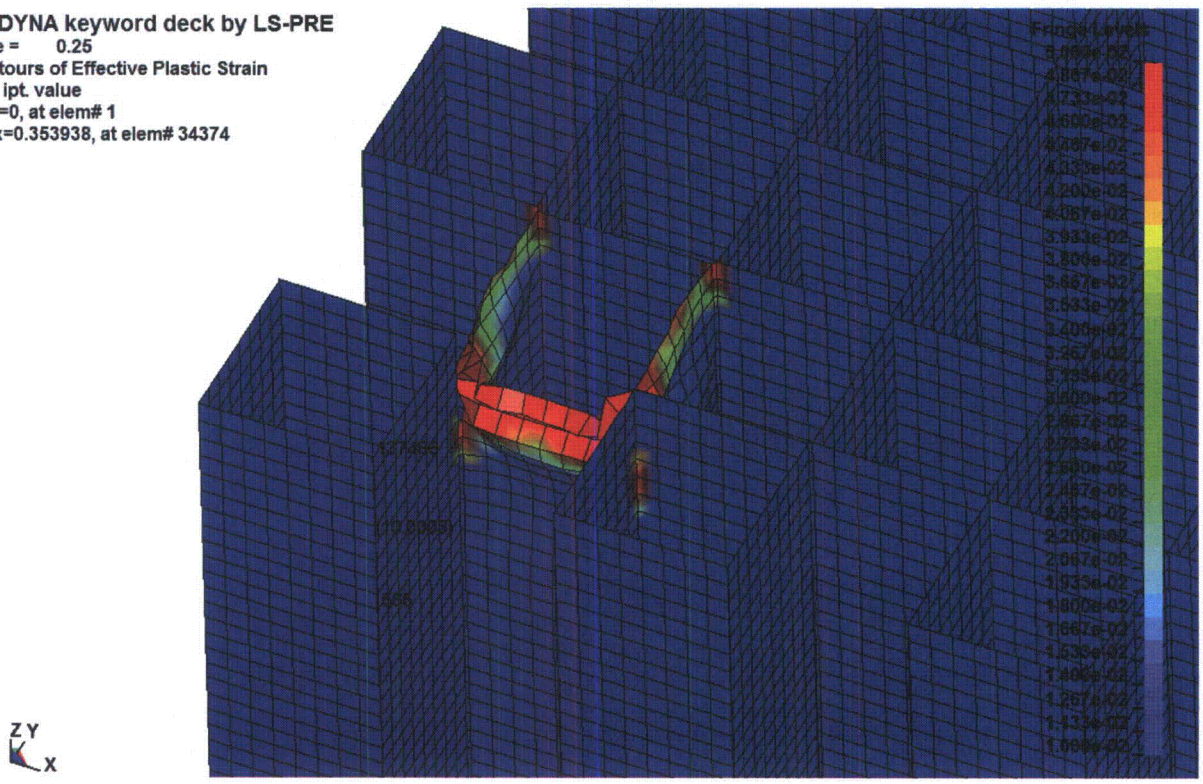

Figure 17-7: Deformed Shape of Spent Fuel Rack Due to Interior Cell Impact

Table 17-3 RESULTS FOR FUEL ASSEMBLY DROP ONTO INTERIOR CELL	
Impact Duration (sec)	0.095
Peak Impact Force (lbf)	32,915
Fuel Assembly Vertical Displacement (in)	3.15
Plastic Deformation Measured from the Rack Top (in)	10.0

The LS-DYNA analysis results demonstrate that the plastic deformation in the rack cell walls resulting from a shallow drop accident (onto a perimeter cell or an interior cell) does not extend down into the neutron absorber zone, which is defined as the vertical length of the cell blanketed by the fixed neutron absorber panel. For the BVPS-2 spent fuel racks, the minimum distance from the top of the rack to the top edge of the neutron absorber panel (the neutron absorber zone) is 19.75 inches. From the LS-DYNA simulations, the dropped fuel assembly moves downward crushing the impacted cell wall to a maximum depth of 3.15 inches (interior cell drop), and the plastic strain in the impacted cell wall diminishes to zero at a distance of 12 inches (perimeter cell drop) below the top of the rack (Figure 17-4). Since the depth of damage by either measure is less than 19.75 inches, the neutron absorber panels do not suffer any damage, and therefore the shallow drop accident has no adverse effect on the criticality safety analysis for the BVPS-2 spent fuel racks. In fact, the criticality safety analysis takes no credit for the uppermost 1.3 inches of neutron absorber length, which extends above the active fuel region (assuming the maximum active fuel height and worst-case tolerances). Therefore, taking into consideration the criticality safety analysis, the more precise limit on the permanent deformation to the spent fuel rack due to a shallow drop accident is no greater than 21.05 inches (19.75 inches plus 1.3 inches) measured from the top of the rack. Based on this criterion, the minimum computed safety factor for the shallow drop accident is:

$$SF = \frac{21.05"}{12"} = 1.75$$

Per Table 1 of Appendix D to SRP 3.8.4, the acceptance limit for fuel drop accidents (load combination D + L + F_d) is stated as, "The functional capability of the fuel racks should be demonstrated." Since the basic function of the fuel racks is to maintain the fuel in a sub-critical storage configuration, and the shallow fuel drop accident does not adversely affect the criticality safety of the racks as demonstrated above, the proposed rack design meets the required acceptance limit for this accident event.

Supplement to RAI-19

1. Please confirm that concrete properties utilized in the proposed reracking LAR are in compliance with the BVPS-2 licensing basis. To completely respond to this RAI, the staff requests that the licensee confirm that the concrete properties (compressive strength, elastic modulus, etc.) used in all evaluations/calculations performed for the proposed BVPS-2 reracking are in accordance with the BVPS-2 licensing basis.

Response:

The structural calculations have been confirmed or revised where necessary to use the minimum concrete compressive strength defined in UFSAR Section 3.8.4.6. The following properties are per the licensing basis.

Concrete compressive strength: $f_c' = 3000 psi$

Elastic modulus (from ACI 318-71, Section 8.3 Modulus of Elasticity):

$$Ec = 57000\sqrt{f_c'} = 57000\sqrt{3000 psi} = 3122019\, lb/in^2$$

2. The August 9, 2010 supplemental response provided a table summarizing the results of 3000 psi run for rack drop.

a) For 3000 psi run, the strain in the liner plate is reported as 0.0088 and the impact force on the floor is reported as 159 kips. For the 4000 psi case, the strain in the liner plate was reported as 0.052 and the impact force on the floor was reported as 156.09 kips (624.36/4). The value of the liner plate strain for the 4000 psi case is 6 times larger than the strain value reported for the 3000 psi case. Considering the comparable values of the impact force on the floor for both the 3000 and 4000 psi cases, please provide further discussion to clarify why the strain values are so far apart.

Response:

The reason that the plastic strain in the liner decreased by a factor of 6, despite the fact that the concrete compressive strength was decreased from 4,000 psi to 3,000 psi, is because the contact damping at the rack/SFP liner interface was also increased from 0% to 20% in conjunction with the change in compressive strength. The original rack drop analysis, which utilized 4,000 psi concrete, conservatively assumed 0% contact damping. When the analysis was re-performed using 3,000 psi concrete, the contact damping was set to 20% (which is the recommended value per the LS-DYNA user manual for impact simulations) to obtain a more realistic solution. This change,

however, was not explained to the NRC Staff in the previous RAI response, which was submitted on August 9, 2010. To the contrary, the RAI response incorrectly stated: "Apart from the change in concrete strength, no other changes to the LS-DYNA simulation model have been made." It is also noted that the time step reduction factor was decreased from 0.9 to 0.8 in the revised LS-DYNA analysis to ensure a converged solution for the reduced strength concrete. This change, however, had only a minor effect on the results as compared to the change in contact damping. Both Holtec and FENOC have entered this occurrence into their respective corrective action programs.

To resolve this issue, the rack drop analysis has been re-performed using 3,000 psi concrete, 0% contact damping, and a time step reduction factor of 0.9, so that the only change to the LS-DYNA model (relative the original simulation) is the concrete compressive strength (Simulation No. 3). The following table summarizes the key input parameters and the key results for the three "local" rack drop simulations that have been performed.

	Simulation No. 1	Simulation No. 2	Simulation No. 3
Concrete compressive strength, psi	4,000	3,000	3,000
Contact damping percentage	0	20	0
Time step reduction factor	0.9	0.8	0.9
Impact duration, sec	0.062	0.062	0.064
Peak impact force on SFP floor, lbf	156,090	159,000	157,150
Maximum plastic strain in SFP liner	0.0524	0.0088	0.0542
Number of plastically deformed cells near pedestal	8	8	8

From the above table, when the only change to the LS-DYNA model is a reduction in the concrete compressive strength from 4,000 psi (Simulation No. 1) to 3,000 psi (Simulation No. 3), there is a slight increase in the maximum plastic strain in the SFP liner from 0.0524 to 0.0542, as expected. This is because the dropped rack indents deeper into the 3,000 psi concrete slab and, therefore, produces more strain in the SFP liner. When contact damping is introduced (Simulation No. 2), the plastic strain in the liner reduces significantly. The impact duration and the peak impact force are much less sensitive to the concrete compressive strength and the contact damping

within the range of values considered. The most important observation from the above table is that the maximum plastic strain in the SFP liner from all three simulations is well below the failure strain limit of the material (SA-240 304), which conservatively assuming a triaxial factor of 0.5 for biaxial tension is at least greater than 0.362 (failure strain limit for SA-240 304L material discussed in RAI 17, page 38). Therefore, the postulated rack drop event will not cause a breach in the SFP liner leading to an uncontrollable loss of SFP water.

b) Furthermore, the impact duration is reported as 0.62 seconds. Please confirm that 0.62 seconds is the correct value for the impact duration.

Response:

There was a typographical error in the previous response, which was submitted to the NRC on August 9, 2010. The impact duration should have been reported as 0.062 seconds (as shown in the above table), not 0.62 seconds. FENOC has entered this occurrence into their corrective action program.